A cleaved METTL3 potentiates the METTL3-WTAP interaction and breast cancer progression

Chaojun Yan [1, 5], Jingjing Xiong [1, 5], Zirui Zhou[1, 5], Qifang Li[1, 5], Chuan Gao[1], Mengyao Zhang[1], Liya Yu[1], Jinpeng Li[2], Ming-Ming Hu[3], Chen-Song Zhang[4], Cheguo Cai[1], Haojian Zhang[3] and Jing Zhang[1*]

[1]Department of Thyroid and Breast Surgery, Medical Research Institute, Frontier Science Center for Immunology and Metabolism, Zhongnan Hospital of Wuhan University, Wuhan University, Wuhan, 430071, China

[2]Department of Thyroid and Breast Surgery, Zhongnan Hospital of Wuhan University, Wuhan, 430071, China

[3]Department of Infectious Diseases, Medical Research Institute, Frontier Science Center for Immunology and Metabolism, Zhongnan Hospital of Wuhan University, Wuhan University, Wuhan, 430071, China

[4]State Key Laboratory for Cellular Stress Biology, Innovation Center for Cell Signaling Network, School of Life Sciences, Xiamen University, Fujian, 361102, China

[5]These authors contributed equally

*Corresponding author. Tel: +86-18062556849; Email: Jing_Zhang@whu.edu.cn (J.Z.)

Abstract

N^6-methyladenosine (m^6A) methylation of RNA by the methyltransferase complex (MTC), with core components including METTL3-METTL14 heterodimers and *Wilms' tumor 1-associated protein* (WTAP), contributes to breast tumorigenesis, but the underlying regulatory mechanisms remain elusive. Here, we identify a novel cleaved form METTL3a (residues 239-580 of METTL3). We find that METTL3a is required for the METTL3-WTAP interaction, RNA m^6A deposition, as well as cancer cell proliferation. Mechanistically, we find that METTL3a is essential for the METTL3-METTL3 interaction, which is a prerequisite step for recruitment of WTAP in MTC. Analysis of m^6A sequencing data shows that depletion of METTL3a globally disrupts m^6A deposition, and METTL3a mediates mTOR activation via m^6A-mediated suppression of TMEM127 expression. Moreover, we find that METTL3 cleavage is mediated by proteasome in an mTOR-dependent manner, revealing positive regulatory feedback between METTL3a and mTOR signaling. Our findings reveal METTL3a as an important component of MTC, and suggest the METTL3a-mTOR axis as a potential therapeutic target for breast cancer.

Keywords: METTL3, methyltransferase complex (MTC), m^6A methylation, breast tumorigenesis

Introduction

N6-methyladenosine (m^6A) methylation is the most abundant and evolutionarily conserved internal mRNA modification in eukaryotes, and is involved in numerous aspects of mRNA metabolism including RNA splicing, localization, stability, and translation (Huang et al., 2020; KD et al., 2015; Li et al., 2017a; Lin et al., 2016; Xiao et al., 2016). m^6A mRNA modification participates in numerous physiological processes, such as neurogenesis (Li et al., 2017b; Li et al., 2018b; Livneh et al., 2020; Wang et al., 2018; Yoon et al., 2017), embryo development (Batista et al., 2014; Li et al., 2018a; Mendel et al., 2018; Wang et al., 2014), and reproductive system development (Haussmann et al., 2016; Ivanova et al., 2017; Kasowitz et al., 2018; Xia et al., 2018; Zheng et al., 2013). Dysregulation of m^6A deposition is associated with various diseases including cancer pathogenesis and drug resistance (Huang et al., 2020; Lan et al., 2021; Zhang et al., 2021), such as the core m^6A methyltransferase (METTL3) promotes the progression of breast cancer through elevating expression of mammalian hepatitis BX-interacting protein and inhibiting tumor suppressor *let-7g* (Cai et al., 2018), inhibits tumor immune surveillance by upregulating PD-L1 mRNA level (Wan et al., 2022), and contributes to breast cancer tamoxifen resistance by upregulation of AK4 expression (Liu et al., 2020).

The m^6A mRNA modification is deposited by a methyltransferase complex (MTC), the METTL3-METTL14-WTAP complex serves as the core of MTC, METTL3 is the core catalytic component, METTL14 contributes to substrate RNA recognition, triggering METTL3 methylation activity (Huang et al., 2019; Wang et al., 2016a; Wang et al., 2016b; Wang et al., 2014), and WTAP has been recognized as an essential adaptor responsible for recruitment of METTL3-METTL14 heterodimer to nuclear speckles. The m^6A modifications are globally reduced in the absence of WTAP (Liu et al., 2014; Ping et al., 2014). The underlying regulatory mechanisms of m^6A machinery have recently begun to emerge. In particular, ERK was found to phosphorylate METTL3 and WTAP, resulting in stabilization of the m^6A methyltransferase complex (Sun et al., 2020a). Three other studies reported that mTORC1 promotes WTAP translation (Cho et al., 2021), S-adenosylmethionine (SAM) synthesis (Villa et al., 2021), and activation of chaperonin CCT complex (Tang et al., 2021), leading to the global increase in m^6A modifications. In this study, we have identified a cleaved form of METTL3, METTL3a (residues 239-580), that is essential for the METTL3-WTAP interaction, RNA m^6A methylation, and breast cancer progression.

Results

Identification of two novel C-terminal short forms METTL3a (residues 239-580) and METTL3b (residues 197-580)

METTL3 is well-known to promote breast tumorigenesis (Huang et al., 2020). We obtained breast cancer patient tumor tissues and found that METTL3 was upregulated in tumor samples (Figure 1A). Notably, we observed two short bands, which were all elevated synchronously with the full-length (FL) of METTL3. To determine whether these bands were derived from METTL3, we constructed METTL3 knockdown in human T47D breast cancer cell lines by METTL3 shRNA and found that the amount of these two short bands was abolished (Figure 1B). Reconstitution of exogenous METTL3 by no tagged pMSCV-METTL3 construct in these cells rescued the expression levels of these two bands (Figure 1C). Interestingly, we observed that the two short bands were recognized by antibody against the C-terminal, but not N-terminal of METTL3 (Figure 1B), suggesting that these short forms are derived from the C-terminal of METTL3. Furthermore, we constructed T47D cell line stably expressing exogenous METTL3 by using C-terminal Flag-tagged pMSCV-METTL3 plasmid and also observed these short

bands by Flag antibody (Figure 1D). These results indicate that these short bands are METTL3 C-terminal short forms, and we designated these two short forms as METTL3a and METTL3b as indicated in the Figures.

Since both endogenous and exogenous METTL3 expression in cells could generate METTL3a and METTL3b, we hypothesized that they are most likely generated from post-translational regulation. To test this possibility, we purified recombinant protein of METTL3 and incubated it with T47D cell lysates, and found that the purified METTL3-His could generate these short forms upon incubation with T47D cell lysates (Figure 1E). This result indicates that these short forms are derived from post-translational products of METTL3. To determine the specific METTL3 regions contained in these short forms, we separated each clean short form through SDS-PAGE and *Ponceau S* staining of the purified recombinant METTL3-Flag followed by edman sequencing of their respective first five N-terminal amino acids. The sequencing results showed that the METTL3a N-terminal sequence was $_{239}$SKKVS$_{243}$, while that of METTL3b was $_{197}$GLNSS$_{201}$, revealing that residues 239-580 and 197-580 comprise METTL3a and METTL3b, respectively (Figure 1F). We therefore identified two C-terminal short forms METTL3a (residues 239-580) and METTL3b (residues 197-580).

METTL3a and METTL3b are post-translational products through highly conserved residues

We next generated point mutations or deletions in those conserved terminal residues, which further revealed that deletion of METTL3 Q238 (Δ238) or Q239 (Δ239) could most significantly reduce the expression of METTL3a in 293T cells (Figure 2A, B). Similarly, deletion of L198 (Δ198) or L199 (Δ199) resulted in the strongest suppression of METTL3b expression (Figure 2C, D). Notably, endogenous deletion of either L198 or Q238 (METTL3-Δ238 or METTL3-Δ198) by CRISPR/Cas9 knock-in (KI) could lead to decreased expression of both short forms (Figure 2E, F). Furthermore, we confirmed these post-translationally generated short forms by incubation of purified recombinant METTL3 with cell lysates of T47D, and found that METTL3-WT-His, but not METTL3-(Δ198+Δ238)-His, could generate these short forms (Figure 2G). Collectively, these results suggest that METTL3a and METTL3b are post-translationally generated through the highly conserved residues.

Through immunofluorescence assays, we found that METTL3a, METTL3b, METTL3-Δ198 and METTL3-Δ238 were mainly localized to nucleus, similar to METTL3 WT (Figure supplement 1). And, *in vitro* methylation assays showed that METTL3a, METTL3b, METTL3-Δ198 and METTL3-Δ238, similar to METTL3-WT, showed m^{6}A methyltransferase activity (Figure 2H, I). These data suggest that these METTL3 variants have no effect on METTL3 localization or *in vitro* m^{6}A methyltransferase activity.

It should be mentioned that the strong promoter CMV-driven pHAGE-METTL3-Flag construct used for purification of recombinant METTL3-Flag showed another highly expressed short form, named as METTL3c, which was very close in size to b (Figure supplement 2A). Therefore, we had to exclude METTL3c expression for purification of METTL3b. We thus performed domain mapping for METTL3 with various mutations as indicated to identify conserved residues responsible for the expression of METTL3c, and finally found that point mutations in the M156 and M157 residues to convert these highly conserved amino acids into alanines (2MA) could lead to disappearance of METTL3c (Figure supplement 2B-F). We then used this METTL3-2MA-Flag construct for edman sequencing as described in Figure 2B. METTL3c, which is disappear upon depletion of both M156 and M157, could be a product of an alternative open reading frame rather than a cleavage product, as deletion of the start codon leads to its loss. Since METTL3c was largely absent within endogenous METTL3, combined with data from

m^6A dot blots and tumor cell growth assays showing that METTL3-2MA functioned similarly to METTL3-WT (Figure supplement 2G-K), we did not investigate METTL3c in the following study.

Both METTL3a and full-length METTL3 are required for cell proliferation and breast cancer progression

Since our above data have showed that METTL3a, METTL3b, METTL3-Δ198 and METTL3-Δ238 display the similar distributions with METTL3 WT and also harbor intact m^6A methyltransferase activity *in vitro*, we wondered whether these two short forms, which are upregulated in breast cancer, are functionally important. We therefore reconstituted METTL3-WT, METTL3-Δ238, METTL3-Δ198, METTL3a, or METTL3b respectively in METTL3 knockout (KO) T47D and MDA-MB-231 cell lines (Figure 3A, C). Cell proliferation assays showed that reconstitution with METTL3-WT or METTL3-Δ198, but not METTL3-Δ238, METTL3a or METTL3b, could rescue the defects in cell proliferation caused by METTL3 KO in T47D and MDA-MB-231 cell lines (Figure 3B, D). These findings suggest that the short form METTL3a and full-length of METTL3 are required for tumor cell proliferation, since depletion of either one of them failed to rescue the cell growth defect caused by METTL3 KO. In line with these results, METTL3-Δ238 KI 293T cells displayed decrease in cell proliferation compared to METTL3 WT cells (Figure 3E, F), and reconstitution of METTL3a, but not METTL3b, could rescue the reduced cell proliferation (Figure 3G, H). These data suggest that METTL3a is required for METTL3-mediated regulation of cell proliferation.

Further, we used METTL3-WT, METTL3-Δ238 or METTL3-Δ198 to respectively complement MDA-MB-231 METTL3 KO cells, and injected these cells orthotopically into the mammary fat pads of mice and performed bi-weekly measurement of tumor volume by caliper. Consistent with our *in vitro* results, we observed that reconstitution of either METTL3-WT or METTL3-Δ198 could rescue the METTL3 KO-mediated defect in tumor growth, while expression of METTL3-Δ238 could not (Figure 3I-K). These results suggest that METTL3a is essential for METTL3-mediated regulation of breast cancer progression.

METTL3a is required for the interaction between METTL3 and WTAP

METTL3-mediated tumor cell growth is known to rely on MTC for its methyltransferase activity (Lan et al., 2019). Here, our data showed that either METTL3 with loss of METTL3a (METTL3-Δ238) or METTL3a alone failed to rescue cell proliferation defects coursed by METTL3 KO, although both of them have intact catalytic activity *in vitro*. Therefore, we wondered whether METTL3a participates in the m^6A methyltransferase complex, among which METTL3, METTL14 and WTAP are core components required for intracellular RNA m^6A modification (Liu et al., 2014; Ping et al., 2014). To this end, we performed immunoprecipitation (IP) assays in T47D and 293T cell lines and observed that METTL3-Δ238 had much weaker interaction with WTAP, but retained its interaction with METTL14, whereas METTL3-Δ198 could interact with both WTAP and METTL14 (Figure 4A, B), consistent with the phenotypic study showing that METTL3-Δ238, but not METTL3-Δ198, affected tumor cell proliferation. Previous reports have shown that WTAP interacts with the METTL3 N-terminal leader helix domain (LH, 1-34aa), and that METTL14 can heterodimerize with METTL3 through their individual C-terminal methyltransferase domains (Schöller et al., 2018; Wang et al., 2016a; Wang et al., 2016b). In line with these findings, our results showed that both METTL3a and METTL3b, which lack the METTL3 N-terminal domain, failed to interact with WTAP, but could bind with METTL14 (Figure 4A, B). IP assays in METTL3 knockdown (KD) 293T cells further confirmed the decreased interaction between METTL3-Δ238 and WTAP, and reconstitution with exogenous METTL3a could rescue their

interaction (Figure 4C, D), indicating that METTL3a is required for the METTL3-WTAP interaction.

METTL3a mediates the METTL3-METTL3 interaction, a prerequisite step for WTAP recruitment in MTC complex

Since METTL3a showed no interaction with WTAP, we next sought to determine how reduced expression of METTL3a decreased the METTL3-WTAP interaction. Recent study has shown that METTL3 is capable of self-interaction and undergoes phase separation in nuclei (Han et al., 2022). Consistently, we also found that the METTL3-METTL3 interaction could occur in both 293T cell line and *in vitro* recombinant protein purification-IP systems (Figure 5A, B). And, the METTL3-METTL3 interaction is independent of DNA or RNA (Figure 5C). We further constructed METTL3 N-terminal (1-238) and C-terminal (239-580) truncation plasmids. And, IP assays showed that the METTL3-METTL3 interaction was through its C-terminal domain (Figure 5D-E-figure supplement 3A-C). We therefore wondered whether METTL3a could mediate the METTL3-METTL3 interaction, then affects further recruitment of WTAP. Indeed, we found that the interaction between METTL3-Δ238 and METTL3-Δ238 was barely detectable, but restored under exogenous expression of METTL3a, as was its interaction with WTAP (Figure 5F), suggesting that METTL3a is required for the METTL3-METTL3 interaction, that is a prerequisite step for the METTL3-WTAP interaction. Our finding is in line with previous study showing that WTAP only interacts with METTL3 in dense phase, which is formed by METTL3-METTL3 interaction (Han et al., 2022).

We next examined the intracellular assembly process of MTC. Since METTL3 is the key which functions as methyltransferase, we first determined the effect of METTL3 on the formation of MTC. Through Co-IP assays with 293T cells, we found that METTL3 depletion decreased the METTL14-METTL14 and METTL14-WTAP interactions (Figure 5G), suggesting that the intracellular METTL14-METTL14 and METTL14-WTAP interactions take place at least partially through METTL3. While METTL14 depletion did not reduce, but rather increase the METTL3-METTL3 and METTL3-WTAP interactions (Figure 5H). Recent cryo-EM data demonstrate that WTAP can form dimer (Su et al., 2022). As expected, we observed the WTAP-WTAP interaction in 293T cells, and it was unaffected by depletion of METTL3 (Figure 5I). Conversely, WTAP depletion had no effect on the METTL3-METTL3 and METTL3-METTL14 interactions (Figure 5J, K). Altogether, we conclude that the METTL3-METTL3 interaction acts as a core initiating the formation of METTL3-METTL14-WTAP complex. These data demonstrate that METTL3a mediates the METTL3-METTL3 interactions, thereby forming larger complexes for efficient recruitment of WTAP in MTC.

WTAP is essential for m^6A deposition (Liu et al., 2014; Ping et al., 2014), our current data suggest that METTL3a is required for METTL3-WTAP interaction. We therefore hypothesized that METTL3a may play a role in intracellular RNA m^6A deposition. Through m^6A dot blot assays, we observed that reconstitution of METTL3-Δ238 could not rescue the decreased RNA m^6A modification caused by METTL3 depletion in 293T cells, while reconstitution of METTL3-Δ198 or METTL3-WT in these cells restored the m^6A deposition (Figure 5L, M). Consistently, METTL3-Δ238 KI cells showed reduced m^6A level compared to METTL3-WT cells, and reconstitution of exogenous METTL3a in METTL3-Δ238 KI cells rescued this decrease (Figure 5N, O). Collectively, our data suggest that METTL3a is required for the formation of METTL3-METTL14-WTAP complex and m^6A RNA modification.

METTL3a is essential for the METTL3-mediated m^6A deposition and mTOR activation

In light of our above data showing that METTL3a is required for m^6A RNA methylation, we further

examined how METTL3a affects m^6A RNA modification across the whole genome in T47D cells. To this end, we expressed METTL3-WT, METTL3-Δ198, or METTL3-Δ238 to complement endogenous METTL3 KO T47D cells, then conducted m^6A-seq to identify their differentially modified transcripts. Mapping of transcripts with m^6A modification revealed that m^6A methylation was globally decreased from the transcriptome of METTL3 KO cells expressing empty vector (Vec) or METTL3-Δ238, while the total number of methylation marks was similar among METTL3-Δ198-, METTL3-WT-expressing METTL3 KO cells and the control (sgCtrl+Vec) cells (Figure 6A). Whereas motif analyses of the m^6A peaks showed that the most enriched motif of the transcripts across all groups was the canonical GGAC motif (Figure supplement 4A), and also the distribution of m^6A methylation sites across the full transcriptome were similar among all groups (Figure supplement 4B). To identify their differentially regulated m^6A methylation sites, we first normalized their m^6A peaks with that of METTL3 KO cells expressing vector (sgMETTL3+Vec) to eliminate those peaks not affected by METTL3 KO, we then found that METTL3 KO cells expressing either METTL3-WT or METTL3-Δ198 shared the most of their m^6A peaks (>80%), while those cells expressing METTL3-Δ238 lost 90% of peaks observed in METTL3-WT (Figure 6B). These analyses suggest that downregulation of METTL3a inhibits the METTL3-mediated m^6A deposition.

To explore the potential targets regulated by METTL3a, we analyzed mRNAs associated with differentially regulated m^6A peaks in METTL3-WT- versus METTL3-Δ238-complemented METTL3 KO cells and found that the differentially modified gene transcripts were enriched in several signal transduction pathways, and most highly in the mTOR pathway (Figure 6C). Previous studies have found that METTL3 promotes mTOR activity (Chen et al., 2021; Qin et al., 2021; Sun et al., 2020b), although the underlying mechanism has remained unclear.

In order to verify how METTL3a affects mTOR pathway, we analyzed the m^6A methylome and found that some regulators in the mTOR pathway were methylated in METTL3-WT, but not in METTL3-Δ238 (Figure 6D). Immunoblot analysis of those well-established regulators for mTOR activation showed that TMEM127, a suppressor of mTOR (Qin et al., 2010), was significantly upregulated in METTL3 KO T47D cells (Figure 6E). From m^6A sequencing data, we observed that METTL3 KO led to a significant decrease in m^6A peaks at the 3'UTR of *TMEM127* transcript compared to that in cells reconstituted with METTL3-WT or METTL3-Δ198, but not METTL3-Δ238 (Figure 6F), which was further verified by m^6A RIP assays in T47D and MDA-MB-231 cell lines (Figure 6G-figuer supplement 4C). Subsequent immunoblot assays showed that TMEM127 was negatively regulated by METTL3, and a similar trend with the m^6A-seq data was also observed that METTL3-WT, but not METTL3-Δ238 expression could rescue TMEM127 expression in METTL3 KO T47D and MDA-MB-231 cell lines (Figure 6H-figure supplement 4D). Accordingly, METTL3 KO-mediated decrease in S6K phosphorylation could be rescued by METTL3 WT or METTL3-Δ198, but not by METTL3-Δ238 (Figure 6H-figure supplement 4D). And, knockdown of TMEM127 in the METTL3 depleted T47D cells could restore S6K phosphorylation and cell proliferation (Figure 6I, J). Collectively, our findings demonstrate that METTL3a is required for mTOR activation at least partially through m^6A-mediated suppression of TMEM127 expression, and this modulation contributes to tumor cell proliferation.

Proteasome mediates METTL3 cleavage in an mTOR-dependent manner

In light of our above data showing that the short forms of METTL3 originated through post-translational regulation, we next investigated the mechanism and conditions responsible for processing full-length METTL3 into short forms. It is well known that proteolytic cleavage mediates post-translational process

of protein into small pieces, to identify the potential protease responsible for this process, we screened a series of inhibitors targeting different proteases and found that the proteasomal inhibitors MG132 and Ixazomib could largely block the generation of these short forms (Figure 7A-figure supplement 5A). Proteasome is multi-catalytic protease complex that regulates cellular protein homeostasis through targeted degradation of proteins(Bochtler et al., 1999), and previous work has described the endoproteolytic activity underlying proteasomal function(Baugh and Pilipenko, 2004; Liu et al., 2003; Sorokin et al., 2005). Here, we validated that MG132 treatment could reduce the levels of both endogenous and exogenous short forms of METTL3 in T47D and MDA-MB-231 cell lines (Figure 7B, D). Further, MG132 could also inhibit the *in vitro* proteolytic cleavage of purified recombinant METTL3-His incubated with lysates of T47D cells (Figure 7E). These results suggest that proteasome participates in METTL3 cleavage into the short forms.

Co-immunoprecipitation assays in 293T cells followed by LC-MS/MS showed that METTL3 interacted with the proteasome components PSMC3, PSMC5, and PSMD10 (Figure 7F), which was further confirmed by immunoprecipitation assays targeting METTL3-Flag in T47D cells (Figure 7G). In addition, knockdown of PSMC3, PSMC5 or PSMD10 abrogated the cleavage of METTL3 in MDA-MB-231 cells (Figure 7H-J). As PSMC3, PSMC5 and PSMD10 are all regulatory subunits of 26S proteasome, we hypothesized that 26S proteasome may be responsible for METTL3 cleavage. Indeed, *in vitro* proteasomal cleavage assay by incubation of purified recombinant METTL3 with 26S proteasome showed that 26S proteasome could directly cleave METTL3 WT to METTL3a and METTL3b, while deletion of both L198 and Q238 inhibited this process (Figure 7K). These results support the hypothesis that proteasome is responsible for the cleavage of METTL3 into METTL3a and METTL3b.

mTORC1 promotes the expression of proteasomal subunits (Zhang et al., 2014). We therefore investigated whether mTOR regulates the above proteasome components, and affects METTL3 cleavage. Western blot analysis showed that silence of mTOR in MDA-MB-231 cells inhibited the expression of PSMC3, PSMC5 and PSMD10 (Figure 7L), and also led to decreased accumulation of the METTL3 short forms (Figure 7M). Consistent with this finding, treatment with the mTOR inhibitor rapamycin in T47D and MDA-MB-231 cell lines led to decreased expression of these short forms (Figure 7N). In addition, depletion of either Raptor or Rictor, which are key components of mTOR complex 1 and 2 (mTORC1 and mTORC2), respectively, also reduced the expression of the METTL3 short forms (Figure supplement 5B, C). We also found that cells with constitutively active mTOR signaling due to knockout of *Tsc2,* a negative regulator of mTOR activity (Crino et al., 2006), led to upregulation of these short forms, and proteasome inhibitor MG132 treatment could inhibit this upregulation (Figure 7O), suggesting that mTOR upregulates the METTL3 short forms via proteasome. These cumulative results suggest that proteasome is responsible for METTL3 cleavage, and the mTOR pathway positively regulates this process.

Discussion

In this study, we describe a cleaved form of METTL3, METTL3a, that is essential for the METTL3-WTAP interaction and m^6A deposition, resulting in the promotion of breast tumor progression. Specifically, the cleaved form METTL3a mediates the METTL3-METTL3 interaction, which is a prerequisite step for WTAP binding with METTL3. Analyses of the RNA m^6A methylome reveal that METTL3a is required for the global METTL3-mediated m^6A modification and mTOR activation. Further, we find that the mTOR pathway positively regulates the expression of proteasome components that mediate proteasomal cleavage of METTL3 into METTL3a. These findings reveal a positive feedback

between METTL3a and the mTOR signaling pathway (Figure 7P).

The methyltransferase complex (MTC) mediates m^6A deposition. It is well-established that the core components of the MTC include heterodimers of the METTL3-METTL14 methyltransferases with an adaptor protein WTAP. Here, we found that METTL3 undergoes METTL3-METTL3 interaction which is required for recruitment of WTAP in MTC. Downregulation of METTL3a leads to decrease in both METTL3-METTL3 interaction and the METTL3-WTAP interaction, and consequently attenuates m^6A modification. Based on this work, we propose that METTL3a acts as a bridge between the METTL3-METTL14 heterodimers through mediating the METTL3-METTL3 interaction, thereby resulting in the formation of larger complexes which can efficiently recruit WTAP in MTC. Our finding is in line with previous report showing that METTL3 undergoes self-interaction (Han et al., 2022). In contrast to the constitutive binding of METTL14 to METTL3 in both the diffuse and the dense phase, WTAP only interacts with METTL3 in dense phase (Han et al., 2022), it means that WTAP tends to bind to larger METTL3-METTL14 complexes, which supports our conclusion. It is also noteworthy that METTL3b contains the region of residues 239-580 but is not required for the METTL3-WTAP interaction. Based on our findings, we are inclined to speculate that the cleavage product METTL3a is a structurally appropriate (i.e., small enough) component involved in MTC complex, whereas the METTL3b is not.

Screening of a proteasome inhibitor library in conjunction with LS-MS/MS, we found that the proteasome is responsible for METTL3 cleavage, and deletion of the proteasome components PSMC3, PSMC5 or PSMD10 attenuates the accumulation of cleaved forms of METTL3. Furthermore, we showed that the mTOR pathway promotes this process through positive regulation of proteasomal components. The proteasome is essential for degradation of intracellular proteins, including misfolded mutant and damaged proteins (Bochtler et al., 1999). In addition, proteasome also exhibits endoproteolytic activity (Liu et al., 2003), such as proteasome-mediated cleavage of translation initiation factors eIF4G and eIF3a differentially affects the assembly of ribosomal preinitiation complexes and thus inhibits the translation of viral RNA (Baugh and Pilipenko, 2004), and proteasomal cleavage of the Y-box-binding protein 1 splits off the C-terminal fragment which can translocate into nucleus and participate in cellular adaptation to DNA damage stress (Sorokin et al., 2005), which are similar to METTL3 cleavage identified in this work. Our data indicate that deletion of METTL3 residues L198 or Q238 does not completely block the formation of their respective short forms, leading us to speculate that the proteasome may recognize a conserved motif that likely contains multiple amino acids.

Other recent studies have demonstrated that mTOR increases global m^6A modification by promoting WTAP translation (Cho et al., 2021), S-adenosylmethionine (SAM) synthesis (Villa et al., 2021), and by activating the chaperonin CCT complex (Tang et al., 2021). Here, we reveal a new mechanism by which mTOR promotes the cleavage of METTL3 through positive regulation of proteasome components, thereby enhancing global m^6A deposition. METTL3-mediated tumorigenesis largely relies on its methyltransferase activity. The recent identification of a selective inhibitor of METTL3 catalytic activity that dramatically decreases tumor growth in mouse AML models suggests that m^6A methylation by METTL3 could serve as a promising therapeutic target for cancer treatment (Yankova et al., 2021). Here, we show that the cleaved form METTL3a plays a key role in m^6A methylation activity, thus providing another potential anti-cancer therapeutic approach through blockade of METTL3 cleavage. Several studies have demonstrated that proteasomal activity is upregulated in various cancers (Arlt et al., 2009; Chen and Madura, 2005), and several proteasome inhibitors have received regulatory approval and are routinely used in clinical settings (Manasanch and Orlowski, 2017). Our study expands the rationale for targeting the mTOR-proteasome axis in breast cancer therapies.

Previous studies have reported that METTL3 activates mTOR (Chen et al., 2021; Qin et al., 2021; Sun et al., 2020b), although the underlying mechanism has remained poorly defined. KEGG analysis of transcriptome-wide m^6A sequencing data showed that the mTOR pathway is the most highly enriched signal transduction pathway affected by METTL3a depletion. Furthermore, we show that *TMEM127* is the primary target of METTL3 among those genes involved in the mTOR pathway, and depletion of METTL3a decreases m^6A modification of the *TMEM127* 3'UTR, leading to elevated TMEM127 expression. TMEM127 serves as a suppressor of the mTOR pathway by interfering with mTOR accessibility for its regulators (Qin et al., 2010; Yao et al., 2010). Thus, mechanistically, METTL3a functions as a positive regulatory feedback for activation of the mTOR pathway.

In summary, this study represents the first description to our knowledge of cleaved forms of METTL3, with METTL3a in particular serving as an essential component of the MTC complex, and elucidates the intracellular assembly process of the METTL3-METTL14-WTAP complex. These findings also uncover a positive regulatory feedback between METTL3a and the mTOR pathway which may serve as the basis for development of therapeutic strategies for breast cancer.

Materials and Methods

Cell Culture and Reagents

MDA-MB-231, MEF and 293T cells were cultured in Dulbecco's modified Eagle medium (DMEM, Sigma-Aldrich) containing 10% fetal bovine serum plus 1% penicillin–streptomycin. T47D cells were cultured in RPMI-1640 (Sigma-Aldrich) containing 10% fetal bovine serum with 1% penicillin–streptomycin. Following virus infection, cells were maintained in the presence of G418 (100 μg/mL) or puromycin (2 μg/mL) depending on the vector. All cells were maintained in an incubator at 37 °C and 5% CO_2. Library of enzyme inhibitors were obtained from Selleck. Rapamycin was purchased from Sigma-Aldrich.

Western Blot and Antibodies

EBC buffer (50 mM Tris pH 8.0, 120 mM NaCl, 0.5% NP40, 0.1 mM EDTA and 10% Glycerol) supplemented with complete protease inhibitor (Roche Applied Biosciences) was used to harvest whole cell lysates. Cell lysate concentrations were measured by Bradford assay (Thermo Fisher Scientific), and equal amounts of proteins were loaded onto an SDS-polyacrylamide gel, separated by electrophoresis and blotted onto a nitrocellulose membrane (Milipore). Rabbit METTL3 (86132), HIF-1α (14179), p-S6K (9234), S6K (34475) antibodies were obtained from Cell Signaling Technology. Antibodies against N-terminal METTL3 (A8070), PSMC5 (A1538) were from ABclonal. Mouse Vinculin (V9131) and mouse Flag (F3165) antibody were purchased from Sigma-Aldrich. Antibodies against METTL14 (26158-1-AP), WTAP (mouse, 60188-1-Ig; rabbit, 10200-1-AP), PSMC3 (24142-1-AP), PSMD10 (12342-2-AP), mTOR (66888-1-Ig), TMEM127 (23142-1-AP), Raptor (20984-1-AP), Rictor (27248-1-AP), TSC1 (29906-1-AP), TSC2 (24601-1-AP), LKB1 (10746-1-AP), PIK3CA (27921-1-AP) and rabbit Flag (20543-1-AP) were obtained from Proteintech. Peroxidase-conjugated goat anti-mouse (170-6516) and peroxidase-conjugated goat anti-rabbit (1706515) secondary antibodies were purchased from Bio-Rad.

Plasmids

The cDNA full-length of METTL3 was amplified by PCR and subcloned into lentiviral vector pHAGE or retroviral vector pMSCV containing a C-terminal tag. KOD-Plus Mutagenesis Kit (SMK-101,

TOYOBO) was used to construct METTL3 mutants. All plasmids were sequenced to confirm validity.

siRNAs, lentiviral shRNA, and sgRNA Vectors

Non-targeting siRNA was obtained from Dharmacon (D0012100220) as previous(Zhang et al., 2018). The siRNA target sequence of TMEM127 are as previously described (Qin et al., 2010). Lentiviral short-hairpin RNA (shRNA) against METTL3, METTL14, WTAP, mTOR, Rictor, Raptor, PSMC3, PSMC5 and PSMD10 were obtained by cloning into the pLKO.1 vector. The target sequences for METTL3(CGTCAGTATCTTGGGCAAGTT), METTL14(AAGGATGAGTTAATAGCTAAA, WTAP(AAGGTTCGATTGAGTGAAACA) are as previously described (Xiang et al., 2017). The target sequences (CCGCATTGTCTCTATCAAGTT) for mTOR, Raptor (GGCTAGTCTGTTTCGAA ATTT) and Rictor (ACTTGTGAAGAATCGTATCTT) are as previous reported(Sarbassov et al., 2005). The target sequences for PSMC3, PSMC5 and PSMD10 were obtained from Broad Institute TRC shRNA library. The target sequence are as follows:

shPSMC3-1: CCAAGCCATGAAGGACAAGAT (TRCN0000020229)

shPSMC3-2: CCAGCCCAACACCCAAGTTAA (TRCN0000020231)

shPSMC5-1: CAAGGTTATCATGGCTACTAA (TRCN0000020260)

shPSMC5-2: CAAACAGATCAAGGAGATCAA (TRCN0000020262)

shPSMD10-1: GAGTGCCAGTGAATGATAAAG (TRCN0000374678)

shPSMD10-2: CCGATAAATCCCTGGCTACTA (TRCN0000058073)

The sequence for METTL3 knockout (AGAGTCCAGCTGCTTCTTGT) was as previously described (Xiang et al., 2017).

Virus Production and Infection

293T packaging cell lines were used for lentiviral amplification. Lentiviral infection was carried out as previously described (Zhang et al., 2018). Briefly, lentiviral vector was co-transfected with pSPAX2 and pMD2.G in 293T cells using 40-kDa linearpolyethylenimine (Polysciences, 24,765). Retrovirus generation was by using PLAT-A cells (Cell Biolab). Viruses were collected at 48 h and 72 h post-transfection. After passing through 0.45 μm filters, viruses were used to infect target cells in the presence of 8 μg/mL polybrene (Sigma-Aldrich). Subsequently, target cell lines underwent appropriate antibiotic selection.

Immunoprecipitation

Cells were solubilized with EBC buffer supplemented with complete protease and phosphatase inhibitors (Rhoche Applied Bioscience). Lysates were clarified by centrifugation and then mixed with primary antibodies or anti-Flag M2 beads (Sigma-Aldrich) overnight. Bound complexes were washed with NETN buffer six times and were eluted by boiling in SDS loading buffer. Bound proteins were resolved in SDS-PAGE followed by western blot analysis.

Immunostaining

T47D cells were seeded on glass coverslip. 48 hour later, the cells were fixed with 4% formaldehyde (Sigma-Aldrich) in PBS for 15 min at 37 °C. After being washed with PBS three times, the cells were incubated with PBS plus 0.1% Triton X-100 buffer for 10 min. Next, the cells were blocked with PBS plus 10% FBS at room temperature (RT) for 1 h. Then, cells were incubated with the primary antibody for 2 h at RT and subsequently washed with PBS buffer three times. Then, the cells were incubated with

PBS buffer containing the secondary antibody (Jackson immunoresearch, Cy3 affinipure goat anti-rabbit IgG (H + L), alexa fluor 488 affinipure donkey anti-mouse IgG (H + L) for 1 h in the dark at RT. Finally, the cells were washed three times with PBS, and the slides were analyzed using a Leica confocal microscopy (Leica microsystem, Germany).

Protein expression and purification from 293T cells

Full-length human METTL3-WT or mutant was cloned into pHAGE vector containing C-terminal 3×FLAG. The plasmid was transfected into 293T cells using PEI (Polysciences, high potency linear, MW = 40 000) transfection reagent. Protein purification from 293T cells was previously described(Huang et al., 2021). Briefly, cells were harvested after 36 h transfection and washed three times with cold PBS. Then cells were resuspended with lysis buffer (50 mM HEPES at pH 7.4, 300 mM NaCl, 1 mM EGTA, 0.5% Triton-X 100 and complete protease inhibitor) and incubated on ice for 15 min. Then centrifuged at 14 000 r.p.m. for 20 min at 4 °C, and the supernatant was block with protein G agarose for 1 h at 4 ° C. Next the supernatant was incubated the anti-Flag M2 affinity Gel (Sigma-Aldrich) for 4 h at 4 °C. The gel was washed with three times with lysis buffer and washed twice with wash buffer (50 mM HEPES at pH7.4, 150 mM NaCl, 1 mM EGTA, 0.5% Triton-X 100). Then the IP product was eluted with 3×FLAG peptide. Last the elution products were stored at -80°C or loaded onto an SDS-polyacrylamide gel and blotted onto PVDF membrane (Milipore) and stained with *Ponceau S* for Edman sequencing.

Liquid chromatography and mass spectrometry

The eluate from immunoprecipitation was resolubilized in 8 M urea, then each sample was reduced with 5 mM DTT and alkylated (50 mM IAA, 30 min, room temperature in the dark). After trypsin digestion overnight at 37 °C, the peptide was desalted by using C18 StageTip columns and resolubilized in 0.1% formic acid. The liquid chromatography–tandem mass spectrometry (LC-MS/MS) is equipped with an Easy nLC 1200 (Thermo Scientific) coupled to the QExactive HF (Thermo Scientific). Samples were injected onto an Easy Spray PepMap C18 column (75 μm*150 mm, 3 μm, C18, Dr. Maisch GmbH) and separated over a 120 min method. The gradient for separation consisted of 2–100% buffer B at a 300 nl/min flow rate, where buffer A was 0.1% formic acid in water and buffer B consisted of 0.1% formic acid in ACN. After peptide separation, the QExactive HF was operated in data-dependent mode. Resolution for the precursor scan (m/z 200) was set to 60,000, while MS/MS scans resolution was set to 15,000. Raw data were processed using MaxQuant 1.6.1.0 and MS/MS spectra were correlated against the human Uniprot database (uniprot-Homo sapiens [9606]-192901-20201111.fasta). The mass spectrometry proteomics data have been deposited to the ProteomeXchange Consortium via the PRIDE (Perez-Riverol et al., 2022) partner repository with the dataset identifier PXD036899.

***In vitro* METTL3 cleavage assay**

The expressing of METTL3-His was according to the previous described (Huang et al., 2019). T47D cells were incubated with cold buffer (50 mM HEPS at pH 7.4, 150 mM NaCl, 1 mM DTT) for 15 min at 4°C. And then cells were disrupted by ultrasonication. Cell lysates were obtained by centrifuging twice. Incubations of 1 μg proteins with 10 μl cell lysates were performed at 37 °C for 1 h and reactions were stopped by addition of SDS loading buffer.

Proteolytic Assay

HA-METTL3-Flag protein was purified from 293T by using anti-HA magnetic beads (Sigma Aldrich)

as described in this method. Proteasomal cleavage assay was performed as described(Liu et al., 2003). Briefly, incubations of 1 μg proteins with 0.5 μg 26S proteasome (Lifersensors) were performed at 37 ° C for 1 h in a total volume of 20 μl of buffer B (20 mM Tris-HCl, pH 7.1, 20 mM NaCl, 10 mM $MgCl_2$, 0.25 mM ATP, and 1 mM DTT). Reactions were stopped by addition of SDS loading buffer.

GST protein purification and GST pull-down

Glutathione S-transferase plasmids were transformed with BL21 competent cells. Single colonies were picked from above and cultured in 50 ml LB medium containing ampicillin. After overnight culture, 5 ml LB medium was diluted in 500 ml LB medium for shaking at 37 °C for 2–3 h until OD600 of 0.8–1.0 was reached. 0.2 mM IPTG was added to induce GST protein production at 4°C for 16 h before harvesting pellets. Bacteria lysates were disrupted by the nanodebee homogenizer. Cleared bacteria lysates were purified by using glutathione–Sepharose 4B beads. About 10 μl of GST suspension proteins was incubated with purified protein in 500 μl NETN buffer. After 4 h incubation, bound complexes were washed with NETN buffer 8 times followed by boiling in SDS loading buffer and SDS–PAGE.

Cell Proliferation Assay

Cells were plated in triplicate in 96-well plates (2000 cells/well) in appropriate growth medium. At indicated time points, cells were replaced with 90 μL fresh growth medium supplemented with 10 μL MTT reagents (Promega), followed by incubation at 37 °C for 2 h. OD absorbance values were measured at 490 nm using a 96-well plate reader (Biotech).

Orthotopic Tumor Growth

Six-week-old female nude mice were used for xenograft studies. Approximately 1×10^6 viable MDA-MB-231 breast cancer cells were resuspended in 1: 1 ratio in 50 μl medium and 50 μl matrigel (Corning, 354234) and injected orthotopically into the fourth mammary fat pad of each mouse. After injection, tumor size was measured twice a week using an electronic caliper. Tumor volumes were calculated with the formula: volume = $(L \times W^2)/2$, where L is the tumor length and W is the tumor width measured in millimeters. The total mass of tumors was presented as mean±SEM and evaluated statistically using the unpaired two-tail Student's t-test. All mouse experiments were approved by the Animal Care Committees of Wuhan University Medical Research Institue.

Human tumors

Fresh-frozen samples of breast tumor and their accordingly adjacent normal tissues were obtained from zhongnan hospital of Wuhan University. All experiments involving human samples were conducted in compliance with all relevant ethical regulations and were approved by the Medical Ethics Committees of School of Medicine, Wuhan University.

m^6A dot blot

Total RNA was extracted by using MiniBEST Universal RNA extraction Kit (TaKaRa) according to the manufacturer's instructions and quantified by NanoDrop instruments (ThermoFisher). After denaturation, RNA was dropped onto the Amersham Hybond-N+ membrane (RPN119B, GE Healthcare) and UV crosslinked to the membrane. Then the membrane was blocked 1 h with 5% nonfat milk, and incubated with specific anti-m^6A (1:1000 dilution, Synaptic Systems, 202003) antibody overnight at 4°C. Wash three times with TBST and incubated with HRP-conjugated goat anti-rabbit IgG (Bio-Rad).

556

557 **m^6A methyltransferase activity assay**

558 The *in vitro* methyltransferase activity assay was performed following the published procedure(Liu et al.,
559 2015; Y et al., 2018). Briefly, a typical 50 μl of reaction mixture containing the following components:
560 1.5 nmol RNA probes (probe 1: ACGAGUCCUGGACUGAAACGGACUUGU, probe 2:
561 ACGAGUCCUGGAUUGAAACGGAUUUGU), purified METTL3-WT-Flag, METTL3-Δ198-Flag, or
562 METTL3-Δ238-Flag in combination with purified Flag-METTL14, 1 mM SAM, 80 mM KCl, 1.5 mM
563 $MgCl_2$, 0.2 U/ μl RNasin, 10 mM DTT, 4% glycerol and 15 mM HEPES (pH 7.9). The reaction was
564 incubated at 16 °C for 12 h. The methylation of RNA-probe was measured by dot blot with the m^6A
565 antibody (1:300 dilution, Synaptic Systems, 202003).

566

567 **m^6A-seq**

568 Total RNA was extracted using Trizol reagent (Invitrogen, CA, USA) following the manufacturer's
569 procedure. The total RNA quality and quantity were analysis of Bioanalyzer 2100 and RNA 6000 Nano
570 LabChip Kit (Agilent, CA, USA) with RIN number >7.0. Following purification with poly-T oligo
571 attached magnetic beads (Invitrogen), the poly(A) mRNA fractions is fragmented, and then were
572 subjected to incubated for 2 h at 4℃ with m^6A-specific antibody (No. 202003, Synaptic Systems,
573 Germany). Eluted m^6A-containing fragments (IP) and untreated input control fragments are converted to
574 final cDNA library in accordance with a strand-specific library preparation by dUTP method. Then we
575 performed the paired-end 2×150 bp sequencing on an Illumina Novaseq™ 6000 platform at the LC-BIO
576 Bio-tech ltd (Hangzhou, China) following the vendor's recommended protocol. The data have been
577 deposited in the GEO repository with the accession numbers

578

579 **Gene-specific m^6A qPCR**

580 m^6A qPCR was performed as previous described(Li et al., 2017c). Briefly, total RNA was isolated with
581 MiniBEST Universal RNA extraction Kit (TaKaRa). 500 ng total RNA was saved as input sample, the
582 rest mRNA was used for m^6A-immunoprecipitation. Nearly 200 μg total RNA were incubated with m^6A
583 antibody (No. 202003, Synaptic Systems, Germany) and diluted into 500 μl IP buffer (150 mM NaCl,
584 0.1% NP-40, 10 mM Tris-HCl, pH 7.4, 100 U RNase inhibitor), and then rotated at 4℃ for 2 hours,
585 following mixed with Dynabeads™ M-280 and rotated for another 2 hours. After 4 times washing by IP
586 buffer, the IP portion were eluted with 300 μl Proteinase K buffer (5 mM Tris-HCL pH 7.5, 1 mM EDTA
587 pH 8.0, 0.05% SDS, and 4.2 μl Proteinase K (20 mg/ml)) for 1.5 h at 50℃(Meyer et al., 2012), and RNA
588 was recovered with phenol:chloroform extraction followed by ethanol precipitation. The final RNA was
589 reverse transcribed by using ReverTra Ace qPCR RT Kit (TOYOBO). The *TMEM127* mRNA level was
590 determined by the number of amplification cycles (Cq). The relative m^6A levels in *TMEM127* were
591 calculated by the m^6A levels (m^6A IP) normalized using the expression of Input. The qPCR primer are
592 as follows:

593 5'-AATTCAGCCAGACCCAGAGC-3', 5'-GCATCAGACCCACACTGTCA-3'

594

595 **Bioinformatics analyses**

596 Raw sequencing files were filtered using cutadapt (v1.18), and then aligned against the human reference
597 genome (GRCh38/hg38) using tophat (v2.1.1)(Kim et al., 2013). The m^6A-enriched regions in each m^6A-
598 immunoprecipitation sample were identified by MACS2 (v2.2.6) with the option of "--nomodel" with
599 corresponding input library as control(Zhang et al., 2008). Peaks identified with $p < 1e-10$ were used for

downstream analysis. Tracks of signal were computed using MACS2 bdgcmp module with parameter '-m FE', and then visualized using the Integrative Genomics Viewer (IGV) visualization tool (v2.4.14). Peak annotation and motif search were both accomplished using the software HOMER (v4.11)(Heinz et al., 2010). De novo motifs with 6bp length were detected within 100bp around m^6A peak summits identified by MACS2. Differential m^6A modified peaks were identified using exomePeak2 (v1.6.1) ($p < 0.05$). Metagene analysis of m^6A distribution on transcripts was performed using the MetaPlotR pipeline. GO term enrichment analysis was performed by R packages clusterProfiler (v3.8.1)(Wu et al., 2021). The enriched GO terms were further subjected to the web tool REVIGO with the default parameter to filter redundant terms(Supek et al., 2011).

Statistical Analysis

Unpaired two-tailed student's *t*-test was used for experiments comparing two sets of data. Data represent mean ± SEM from three independent experiments. *, **, and *** denote *P* value of <0.05, 0.01, and 0.001, respectively. ns denotes no significance.

Data Availability

The m^6A-seq data have been deposited in the GEO repository under the accession numbers GEO (GSE213727) and the password (sbmbiyakxzyxpor) (https://www.ncbi.nlm.nih.gov/geo/query/acc.cgi?acc=GSE213727).

The LC-MS/MS data have been deposited in ProteomeXchange with identifier (PXD036899) (http://proteomecentral.proteomexchange.org/dataset/PXD036899). The username and code for reviewers are as follows:

Username: reviewer_pxd036899@ebi.ac.uk;

Password: FFHLPfBO

Acknowledgments

The authors thank members of our laboratory for helpful discussions. We thank Dr. Qing Zhang (University of Texas Southwestern), Dr. Pengda Liu (University of North Carolina at Chapel Hill), Dr. Kai Jiang (Wuhan University), Dr. Rui Xiao (Wuhan University), Dr. Yanxun Yu (Wuhan University), Dr. Youngnam Jin (Wuhan University), Dr. Ying Zhang (Wuhan University) and Dr. Xiaodong Zhang (Wuhan University) for critical readings and helpful suggestions. The authors thank Dr. Hong-Bing Shu (Wuhan University) for providing pMSCV emptor vector and METTL14 plasmids and Dr. Chen-Song Zhang (Xiamen University) for providing *Tsc2*-/- MEF cells.

This work was supported by the Fundamental Research Funds for the Central Universities [2042020kf0197 to J.Z.]; National Natural Science Foundation of China [31970737 to J.Z. and 32100570 to C.Y.]; the Startup Funding from Wuhan University [to J.Z.]; Natural Science Foundation of Hubei Province [2020CFA071 and 2022CFA008 to J.Z.]; the National Key Research and Development Program of China [2022YFA1305400 to J.Z.]; and the China Postdoctoral Science Foundation [2020M672408 to C.Y.]. We also sincerely thank the core facility of the Medical Research Institute at Wuhan University for their technical support.

Author contributions

J.Z. conceived and supervised the project. J.Z. and C.Y. analyzed the data. C.Y., J.X., Z.Z. and Q.L. performed most of experiments, M.Z. helped with plasmid construction, L.Y. helped with animal

experiment. C.G. performed bioinformatics analyses. J.L., M.H., C.C., C.Z. and H.Z. provided essential reagents and key advices on the project. J.Z. and C.Y. wrote the paper with critical comments from all authors.

Conflict of interest

The authors declare no potential conflicts of interest.

References

Arlt, A., Bauer, I., Schafmayer, C., Tepel, J., Muerkoster, S.S., Brosch, M., Roder, C., Kalthoff, H., Hampe, J., Moyer, M.P., Folsch, U.R., and Schafer, H. (2009). Increased proteasome subunit protein expression and proteasome activity in colon cancer relate to an enhanced activation of nuclear factor E2-related factor 2 (Nrf2). Oncogene *28*, 3983-3996. doi.org/10.1038/onc.2009.264.

Batista, P.J., Molinie, B., Wang, J., Qu, K., Zhang, J., Li, L., Bouley, D.M., Lujan, E., Haddad, B., Daneshvar, K., Carter, A.C., Flynn, R.A., Zhou, C., Lim, K.S., Dedon, P., Wernig, M., Mullen, A.C., Xing, Y., Giallourakis, C.C., and Chang, H.Y. (2014). m(6)A RNA modification controls cell fate transition in mammalian embryonic stem cells. Cell Stem Cell *15*, 707-719. doi.org/10.1016/j.stem.2014.09.019.

Baugh, J.M., and Pilipenko, E.V. (2004). 20S proteasome differentially alters translation of different mRNAs via the cleavage of eIF4F and eIF3. Molecular cell *16*, 575-586. doi.org/10.1016/j.molcel.2004.10.017.

Bochtler, M., Ditzel, L., Groll, M., Hartmann, C., and Huber, R. (1999). The proteasome. Annual review of biophysics and biomolecular structure *28*, 295-317. doi.org/10.1146/annurev.biophys.28.1.295

Cai, X., Wang, X., Cao, C., Gao, Y., Zhang, S., Yang, Z., Liu, Y., Zhang, X., Zhang, W., and Ye, L. (2018). HBXIP-elevated methyltransferase METTL3 promotes the progression of breast cancer via inhibiting tumor suppressor let-7g. Cancer Lett *415*, 11-19. doi.org/10.1016/j.canlet.2017.11.018.

Chen, H., Gao, S., Liu, W., Wong, C.C., Wu, J., Wu, J., Liu, D., Gou, H., Kang, W., Zhai, J., Li, C., Su, H., Wang, S., Soares, F., Han, J., He, H.H., and Yu, J. (2021). RNA N(6)-Methyladenosine Methyltransferase METTL3 Facilitates Colorectal Cancer by Activating the m(6)A-GLUT1-mTORC1 Axis and Is a Therapeutic Target. Gastroenterology *160*, 1284-1300 e1216. doi.org/10.1053/j.gastro.2020.11.013.

Chen, L., and Madura, K. (2005). Increased proteasome activity, ubiquitin-conjugating enzymes, and eEF1A translation factor detected in breast cancer tissue. Cancer Res *65*, 5599-5606. doi.org/10.1158/0008-5472.CAN-05-0201.

Cho, S., Lee, G., Pickering, B.F., Jang, C., Park, J.H., He, L., Mathur, L., Kim, S.S., Jung, S., Tang, H.W., Monette, S., Rabinowitz, J.D., Perrimon, N., Jaffrey, S.R., and Blenis, J. (2021). mTORC1 promotes cell growth via m(6)A-dependent mRNA degradation. Molecular cell *81*, 2064-2075 e2068. doi.org/10.1016/j.molcel.2021.03.010.

Crino, P.B., Nathanson, K.L., and Henske, E.P. (2006). The tuberous sclerosis complex. New England Journal of Medicine *355*, 1345-1356

Han, D., Longhini, A.P., Zhang, X., Hoang, V., Wilson, M.Z., and Kosik, K.S. (2022). Dynamic assembly of the mRNA m6A methyltransferase complex is regulated by METTL3 phase separation. PLoS Biol *20*, e3001535. doi.org/10.1371/journal.pbio.3001535.

Haussmann, I.U., Bodi, Z., Sanchez-Moran, E., Mongan, N.P., Archer, N., Fray, R.G., and Soller, M. (2016). m(6)A potentiates Sxl alternative pre-mRNA splicing for robust Drosophila sex determination.

Nature *540*, 301-304. doi.org/10.1038/nature20577.
Heinz, S., Benner, C., Spann, N., Bertolino, E., Lin, Y.C., Laslo, P., Cheng, J.X., Murre, C., Singh, H., and Glass, C.K. (2010). Simple combinations of lineage-determining transcription factors prime cis-regulatory elements required for macrophage and B cell identities. Molecular cell *38*, 576-589. doi.org/10.1016/j.molcel.2010.05.004.
Huang, H., Weng, H., and Chen, J. (2020). m(6)A( )Modification in Coding and Non-coding RNAs: Roles and Therapeutic Implications in Cancer. Cancer cell *37*, 270-288. doi.org/10.1016/j.ccell.2020.02.004.
Huang, J., Dong, X., Gong, Z., Qin, L.-Y., Yang, S., Zhu, Y.-L., Wang, X., Zhang, D., Zou, T., Yin, P., and Tang, C. (2019). Solution structure of the RNA recognition domain of METTL3-METTL14 N-6-methyladenosine methyltransferase. Protein & Cell *10*, 272-284. doi.org/10.1007/s13238-018-0518-7.
Huang, J.J., Liang, Z.B., Guan, C.R., Hua, S.S., and Jiang, K. (2021). WDR62 regulates spindle dynamics as an adaptor protein between TPX2/Aurora A and katanin. Journal of Cell Biology *220*. doi.org/ARTN e20200716710.1083/jcb.202007167.
Ivanova, I., Much, C., Di Giacomo, M., Azzi, C., Morgan, M., Moreira, P.N., Monahan, J., Carrieri, C., Enright, A.J., and O'Carroll, D. (2017). The RNA m6A reader YTHDF2 is essential for the post-transcriptional regulation of the maternal transcriptome and oocyte competence. Molecular cell *67*, 1059-1067. e1054. doi.org/10.1016/j.molcel.2017.08.003
Kasowitz, S.D., Ma, J., Anderson, S.J., Leu, N.A., Xu, Y., Gregory, B.D., Schultz, R.M., and Wang, P.J. (2018). Nuclear m(6)A reader YTHDC1 regulates alternative polyadenylation and splicing during mouse oocyte development. Plos Genetics *14*. doi.org/10.1371/journal.pgen.1007412.
KD, M., DP, P., J, Z., A, Z., MA, S., O, E., TV, P., SB, Q., and SR, J. (2015). 5' UTR m(6)A Promotes Cap-Independent Translation. Cell *163*, 999-1010. doi.org/10.1016/j.cell.2015.10.012.
Kim, D., Pertea, G., Trapnell, C., Pimentel, H., Kelley, R., and Salzberg, S.L. (2013). TopHat2: accurate alignment of transcriptomes in the presence of insertions, deletions and gene fusions. Genome Biol *14*, R36. doi.org/10.1186/gb-2013-14-4-r36.
Lan, Q., Liu, P.Y., Bell, J.L., Wang, J.Y., Huttelmaier, S., Zhang, X.D., Zhang, L.R., and Liu, T. (2021). The Emerging Roles of RNA m(6)A Methylation and Demethylation as Critical Regulators of Tumorigenesis, Drug Sensitivity, and Resistance. Cancer Research *81*, 3431-3440. doi.org/10.1158/0008-5472.CAN-20-4107.
Lan, Q., Liu, P.Y., Haase, J., Bell, J.L., Huettelmaier, S., and Liu, T. (2019). The Critical Role of RNA m(6)A Methylation in Cancer. Cancer Research *79*, 1285-1292. doi.org/10.1158/0008-5472.can-18-2965.
Li, A., Chen, Y.S., Ping, X.L., Yang, X., Xiao, W., Yang, Y., Sun, H.Y., Zhu, Q., Baidya, P., Wang, X., Bhattarai, D.P., Zhao, Y.L., Sun, B.F., and Yang, Y.G. (2017a). Cytoplasmic m(6)A reader YTHDF3 promotes mRNA translation. Cell Res *27*, 444-447. doi.org/10.1038/cr.2017.10.
Li, L.P., Zang, L.Q., Zhang, F.R., Chen, J.C., Shen, H., Shu, L.Q., Liang, F., Feng, C.Y., Chen, D., Tao, H.K., Xu, T.L., Li, Z.Y., Kang, Y.H., Wu, H., Tang, L.C., Zhang, P.M., Jin, P., Shu, Q.A., and Li, X.K. (2017b). Fat mass and obesity-associated (FTO) protein regulates adult neurogenesis. Human Molecular Genetics *26*, 2398-2411. doi.org/10.1093/hmg/ddx128.
Li, M., Zhao, X., Wang, W., Shi, H., Pan, Q., Lu, Z., Perez, S.P., Suganthan, R., He, C., Bjoras, M., and Klungland, A. (2018a). Ythdf2-mediated m(6)A mRNA clearance modulates neural development in mice. Genome Biol *19*, 69. doi.org/10.1186/s13059-018-1436-y.
Li, M.M., Zhao, X., Wang, W., Shi, H.L., Pan, Q.F., Lu, Z.K., Perez, S.P., Suganthan, R., He, C., Bjoras, M., and Klungland, A. (2018b). Ythdf2-mediated m(6)A mRNA clearance modulates neural development

in mice. Genome Biology *19*. doi. org/ARTN 6910.1186/s13059-018-1436-y.
Li, Z., Weng, H., Su, R., Weng, X., Zuo, Z., Li, C., Huang, H., Nachtergaele, S., Dong, L., Hu, C., Qin, X., Tang, L., Wang, Y., Hong, G.-M., Huang, H., Wang, X., Chen, P., Gurbuxani, S., Arnovitz, S., Li, Y., *et al.* (2017c). FTO Plays an Oncogenic Role in Acute Myeloid Leukemia as a N-6-Methyladenosine RNA Demethylase. Cancer cell *31*, 127-141. doi.org/10.1016/j.ccell.2016.11.017.
Lin, S., Choe, J., Du, P., Triboulet, R., and Gregory, R.I. (2016). The m(6)A Methyltransferase METTL3 Promotes Translation in Human Cancer Cells. Molecular cell *62*, 335-345. doi.org/10.1016/j.molcel.2016.03.021.
Liu, C.W., Corboy, M.J., DeMartino, G.N., and Thomas, P.J. (2003). Endoproteolytic activity of the proteasome. Science (New York, NY) *299*, 408-411. doi.org/10.1126/science.1079293.
Liu, J., Yue, Y., Han, D., Wang, X., Fu, Y., Zhang, L., Jia, G., Yu, M., Lu, Z., Deng, X., Dai, Q., Chen, W., and He, C. (2014). A METTL3-METTL14 complex mediates mammalian nuclear RNA N6-adenosine methylation. Nature chemical biology *10*, 93-95. doi.org/10.1038/nchembio.1432.
Liu, J., Yue, Y., and He, C. (2015). Preparation of Human Nuclear RNA m(6)A Methyltransferases and Demethylases and Biochemical Characterization of Their Catalytic Activity. In Rna Modification, C. He, ed., pp. 117-130. doi.org/10.1016/bs.mie.2015.03.013
Liu, X., Gonzalez, G., Dai, X., Miao, W., Yuan, J., Huang, M., Bade, D., Li, L., Sun, Y., and Wang, Y. (2020). Adenylate kinase 4 modulates the resistance of breast cancer cells to tamoxifen through an m6A-based epitranscriptomic mechanism. Molecular Therapy *28*, 2593-2604. d oi.org/10.1016/j.ymthe.2020.09.007
Livneh, I., Moshitch-Moshkovitz, S., Amariglio, N., Rechavi, G., and Dominissini, D. (2020). The m(6)A epitranscriptome: transcriptome plasticity in brain development and function. Nature reviews Neuroscience *21*, 36-51. doi.org/10.1038/s41583-019-0244-z.
Manasanch, E.E., and Orlowski, R.Z. (2017). Proteasome inhibitors in cancer therapy. Nat Rev Clin Oncol *14*, 417-433
Mendel, M., Chen, K.M., Homolka, D., Gos, P., Pandey, R.R., McCarthy, A.A., and Pillai, R.S. (2018). Methylation of Structured RNA by the m(6)A Writer METTL16 Is Essential for Mouse Embryonic Development. Molecular cell *71*, 986-+. doi.org/10.1016/j.molcel.2018.08.004.
Meyer, K.D., Saletore, Y., Zumbo, P., Elemento, O., Mason, C.E., and Jaffrey, S.R. (2012). Comprehensive Analysis of mRNA Methylation Reveals Enrichment in 3 ' UTRs and near Stop Codons. Cell *149*, 1635-1646. doi.org/10.1016/j.cell.2012.05.003.
Perez-Riverol, Y., Bai, J., Bandla, C., Garcia-Seisdedos, D., Hewapathirana, S., Kamatchinathan, S., Kundu, D.J., Prakash, A., Frericks-Zipper, A., Eisenacher, M., Walzer, M., Wang, S., Brazma, A., and Vizcaino, J.A. (2022). The PRIDE database resources in 2022: a hub for mass spectrometry-based proteomics evidences. Nucleic Acids Res *50*, D543-D552. doi.org/10.1093/nar/gkab1038.
Ping, X.-L., Sun, B.-F., Wang, L., Xiao, W., Yang, X., Wang, W.-J., Adhikari, S., Shi, Y., Lv, Y., Chen, Y.-S., Zhao, X., Li, A., Yang, Y., Dahal, U., Lou, X.-M., Liu, X., Huang, J., Yuan, W.-P., Zhu, X.-F., Cheng, T., *et al.* (2014). Mammalian WTAP is a regulatory subunit of the RNA N6-methyladenosine methyltransferase. Cell Research *24*, 177-189. doi.org/10.1038/cr.2014.3.
Qin, Y., Li, B., Arumugam, S., Lu, Q., Mankash, S.M., Li, J., Sun, B., Li, J., Flavell, R.A., Li, H.B., and Ouyang, X. (2021). m(6)A mRNA methylation-directed myeloid cell activation controls progression of NAFLD and obesity. Cell Rep *37*, 109968. doi.org/10.1016/j.celrep.2021.109968.
Qin, Y., Yao, L., King, E.E., Buddavarapu, K., Lenci, R.E., Chocron, E.S., Lechleiter, J.D., Sass, M., Aronin, N., Schiavi, F., Boaretto, F., Opocher, G., Toledo, R.A., Toledo, S.P.A., Stiles, C., Aguiar, R.C.T.,

and Dahia, P.L.M. (2010). Germline mutations in TMEM127 confer susceptibility to pheochromocytoma. Nature Genetics *42*, 229-233. doi.org/10.1038/ng.533.

Sarbassov, D.D., Guertin, D.A., Ali, S.M., and Sabatini, D.M. (2005). Phosphorylation and regulation of Akt/PKB by the rictor-mTOR complex. Science (New York, NY) *307*, 1098-1101. doi.org/10.1126/science.1106148.

Schöller, E., Weichmann, F., Treiber, T., Ringle, S., Treiber, N., Flatley, A., Feederle, R., Bruckmann, A., and Meister, G. (2018). Interactions, localization, and phosphorylation of the m6A generating METTL3–METTL14–WTAP complex. Rna *24*, 499-512. doi/10.1261/rna.064063.117.

Sorokin, A.V., Selyutina, A.A., Skabkin, M.A., Guryanov, S.G., Nazimov, I.V., Richard, C., Th'Ng, J., Yau, J., Sorensen, P.H., and Ovchinnikov, L.P. (2005). Proteasome-mediated cleavage of the Y-box-binding protein 1 is linked to DNA-damage stress response. The EMBO journal *24*, 3602-3612. doi.org/10.1038/sj.emboj.7600830

Su, S., Li, S., Deng, T., Gao, M., Yin, Y., Wu, B., Peng, C., Liu, J., Ma, J., and Zhang, K. (2022). Cryo-EM structures of human m(6)A writer complexes. Cell Res *32*, 982-994. doi.org/10.1038/s41422-022-00725-8.

Sun, H.L., Zhu, A.C., Gao, Y., Terajima, H., Fei, Q., Liu, S., Zhang, L., Zhang, Z., Harada, B.T., He, Y.Y., Bissonnette, M.B., Hung, M.C., and He, C. (2020a). Stabilization of ERK-Phosphorylated METTL3 by USP5 Increases m(6)A Methylation. Molecular cell *80*, 633-647 e637. doi.org/10.1016/j.molcel.2020.10.026.

Sun, Y., Li, S., Yu, W., Zhao, Z., Gao, J., Chen, C., Wei, M., Liu, T., Li, L., and Liu, L. (2020b). N6-methyladenosine-dependent pri-miR-17-92 maturation suppresses PTEN/TMEM127 and promotes sensitivity to everolimus in gastric cancer. Cell death & disease *11*, 836-836. doi.org/10.1038/s41419-020-03049-w.

Supek, F., Bosnjak, M., Skunca, N., and Smuc, T. (2011). REVIGO Summarizes and Visualizes Long Lists of Gene Ontology Terms. PloS one *6*. doi.org/ARTN e2180010.1371/journal.pone.0021800.

Tang, H.W., Weng, J.H., Lee, W.X., Hu, Y., Gu, L., Cho, S., Lee, G., Binari, R., Li, C., Cheng, M.E., Kim, A.R., Xu, J., Shen, Z., Xu, C., Asara, J.M., Blenis, J., and Perrimon, N. (2021). mTORC1-chaperonin CCT signaling regulates m(6)A RNA methylation to suppress autophagy. Proceedings of the National Academy of Sciences of the United States of America *118*. doi.org/10.1073/pnas.2021945118.

Villa, E., Sahu, U., O'Hara, B.P., Ali, E.S., Helmin, K.A., Asara, J.M., Gao, P., Singer, B.D., and Ben-Sahra, I. (2021). mTORC1 stimulates cell growth through SAM synthesis and m(6)A mRNA-dependent control of protein synthesis. Molecular cell *81*, 2076-2093 e2079. doi.org/10.1016/j.molcel.2021.03.009.

Wan, W.J., Ao, X., Chen, Q., Yu, Y., Ao, L.Q., Xing, W., Guo, W., Wu, X.F., Pu, C.X., Hu, X.T., Li, Z., Yao, M.W., Luo, D.L., and Xu, X. (2022). METTL3/IGF2BP3 axis inhibits tumor immune surveillance by upregulating N-6-methyladenosine modification of PD-L1 mRNA in breast cancer. Molecular Cancer *21*. doi.org/Artn 6010.1186/S12943-021-01447-Y.

Wang, C.X., Cui, G.S., Liu, X.Y., Xu, K., Wang, M., Zhang, X.X., Jiang, L.Y., Li, A., Yang, Y., Lai, W.Y., Sun, B.F., Jiang, G.B., Wang, H.L., Tong, W.M., Li, W., Wang, X.J., Yang, Y.G., and Zhou, Q. (2018). METTL3-mediated m(6) A modification is required for cerebellar development. Plos Biology *16*. doi.org/ARTN e200488010.1371/journal.pbio.2004880.

Wang, P., Doxtader, K.A., and Nam, Y. (2016a). Structural Basis for Cooperative Function of Mettl3 and Mettl14 Methyltransferases. Molecular cell *63*, 306-317. doi.org/10.1016/j.molcel.2016.05.041.

Wang, X., Feng, J., Xue, Y., Guan, Z., Zhang, D., Liu, Z., Gong, Z., Wang, Q., Huang, J., Tang, C., Zou, T., and Yin, P. (2016b). Structural basis of N-6-adenosine methylation by the METTL3-METTL14

complex. Nature *534*, 575-+. doi.org/10.1038/nature18298.

Wang, Y., Li, Y., Toth, J.I., Petroski, M.D., Zhang, Z., and Zhao, J.C. (2014). N-6-methyladenosine modification destabilizes developmental regulators in embryonic stem cells. Nature cell biology *16*, 191-198. doi.org/10.1038/ncb2902.

Wu, T.Z., Hu, E.Q., Xu, S.B., Chen, M.J., Guo, P.F., Dai, Z.H., Feng, T.Z., Zhou, L., Tang, W.L., Zhan, L., Fu, X.C., Liu, S.S., Bo, X.C., and Yu, G.C. (2021). clusterProfiler 4.0: A universal enrichment tool for interpreting omics data. Innovation-Amsterdam *2*. doi.org/Artn 10014110.1016/J.Xinn.2021.100141.

Xia, H., Zhong, C., Wu, X., Chen, J., Tao, B., Xia, X., Shi, M., Zhu, Z., Trudeau, V.L., and Hu, W. (2018). Mettl3 Mutation Disrupts Gamete Maturation and Reduces Fertility in Zebrafish. Genetics *208*, 729-743. doi.org/10.1534/genetics.117.300574.

Xiang, Y., Laurent, B., Hsu, C.H., Nachtergaele, S., Lu, Z., Sheng, W., Xu, C., Chen, H., Ouyang, J., Wang, S., Ling, D., Hsu, P.H., Zou, L., Jambhekar, A., He, C., and Shi, Y. (2017). RNA m(6)A methylation regulates the ultraviolet-induced DNA damage response. Nature *543*, 573-576. doi.org/10.1038/nature21671.

Xiao, W., Adhikari, S., Dahal, U., Chen, Y.-S., Hao, Y.-J., Sun, B.-F., Sun, H.-Y., Li, A., Ping, X.-L., and Lai, W.-Y. (2016). Nuclear m6A reader YTHDC1 regulates mRNA splicing. Molecular cell *61*, 507-519. doi.org/10.1016/j.molcel.2016.01.012

Y, D., G, H., H, Z., J, D., J, H., Y, G., L, L., R, C., Y, W., R, D., J, H., B, J., M, X., J, C., GQ, C., X, Z., and J, Y. (2018). SUMOylation of the m6A-RNA methyltransferase METTL3 modulates its function. Nucleic acids research *46*, 5195-5208. doi.org/10.1093/nar/gky156.

Yankova, E., Blackaby, W., Albertella, M., Rak, J., De Braekeleer, E., Tsagkogeorga, G., Pilka, E.S., Aspris, D., Leggate, D., Hendrick, A.G., Webster, N.A., Andrews, B., Fosbeary, R., Guest, P., Irigoyen, N., Eleftheriou, M., Gozdecka, M., Dias, J.M.L., Bannister, A.J., Vick, B.*, et al.* (2021). Small-molecule inhibition of METTL3 as a strategy against myeloid leukaemia. Nature *593*, 597-601. doi.org/10.1038/s41586-021-03536-w.

Yao, L., Schiavi, F., Cascon, A., Qin, Y., Inglada-Pérez, L., King, E.E., Toledo, R.A., Ercolino, T., Rapizzi, E., Ricketts, C.J., Mori, L., Giacchè, M., Mendola, A., Taschin, E., Boaretto, F., Loli, P., Iacobone, M., Rossi, G.-P., Biondi, B., Lima-Junior, J.V.*, et al.* (2010). Spectrum and Prevalence of FP/TMEM127 Gene Mutations in Pheochromocytomas and Paragangliomas. JAMA *304*, 2611-2619. doi.org/10.1001/jama.2010.1830.

Yoon, K.J., Ringeling, F.R., Vissers, C., Jacob, F., Pokrass, M., Jimenez-Cyrus, D., Su, Y.J., Kim, N.S., Zhu, Y.H., Zheng, L.L., Kim, S., Wang, X.Y., Dore, L.C., Jin, P., Regot, S., Zhuang, X.X., Canzar, S., He, C., Ming, G.L., and Song, H.J. (2017). Temporal Control of Mammalian Cortical Neurogenesis by m(6)A Methylation. Cell *171*, 877-+. doi.org/10.1016/j.cell.2017.09.003.

Zhang, J., Wu, T., Simon, J., Takada, M., Saito, R., Fan, C., Liu, X.D., Jonasch, E., Xie, L., Chen, X., Yao, X.S., Teh, B.T., Tan, P., Zheng, X.N., Li, M.J., Lawrence, C., Fan, J., Geng, J., Liu, X.J., Hu, L.X.*, et al.* (2018). VHL substrate transcription factor ZHX2 as an oncogenic driver in clear cell renal cell carcinoma. Science (New York, NY) *361*, 290-295. doi.org/10.1126/science.aap8411.

Zhang, Y., Chen, W., Zheng, X., Guo, Y., Cao, J., Zhang, Y., Wen, S., Gao, W., and Wu, Y. (2021). Regulatory role and mechanism of m(6)A RNA modification in human metabolic diseases. Molecular therapy oncolytics *22*, 52-63. doi.org/10.1016/j.omto.2021.05.003.

Zhang, Y., Liu, T., Meyer, C.A., Eeckhoute, J., Johnson, D.S., Bernstein, B.E., Nusbaum, C., Myers, R.M., Brown, M., Li, W., and Liu, X.S. (2008). Model-based analysis of ChIP-Seq (MACS). Genome Biol *9*, R137. doi.org/10.1186/gb-2008-9-9-r137.

Zhang, Y., Nicholatos, J., Dreier, J.R., Ricoult, S.J.H., Widenmaier, S.B., Hotamisligil, G.S., Kwiatkowski, D.J., and Manning, B.D. (2014). Coordinated regulation of protein synthesis and degradation by mTORC1. Nature *513*, 440-443. doi.org/10.1038/nature13492.

Zheng, G., Dahl, J.A., Niu, Y., Fedorcsak, P., Huang, C.-M., Li, C.J., Vågbø, C.B., Shi, Y., Wang, W.-L., and Song, S.-H. (2013). ALKBH5 is a mammalian RNA demethylase that impacts RNA metabolism and mouse fertility. Molecular cell *49*, 18-29. doi.org/10.1016/j.molcel.2012.10.015

890

891 ## Figures and figure legends

Figure 1

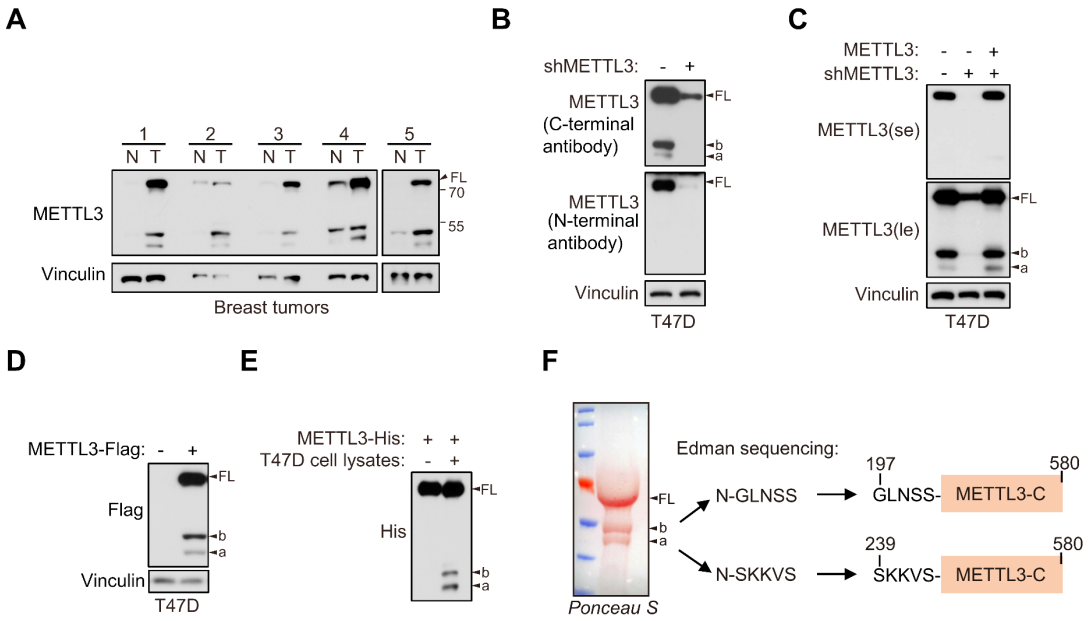

892

893 **Figure 1. Identification of two novel C-terminal short forms of METTL3.**

894 **A** Immunoblot of lysates from paired breast cancer patient non-tumor (N) and tumor (T) tissues.

895 **B** Immunoblot of T47D cells infected with lentivirus encoding METTL3 shRNA or control shRNA by
896 antibodies recognizing N-terminal or C-terminal of METTL3 as indicated.

897 **C** Immunoblot of T47D cells infected with retrovirus encoding shMETTL3 resistant pMSCV-METTL3
898 without tag or control vector followed by METTL3 shRNA or control shRNA infection.

899 **D** Immunoblot of T47D cells infected with retrovirus encoding pMSCV-METTL3 with C-terminal Flag
900 tag.

901 **E** Purified recombinant METTL3-His protein was incubated with or without T47D cell lysates at 37 °C
902 for 1 hour followed by immunoblot with anti-His antibody.

903 **F** *Ponceau S* staining and the N-terminal sequence of the short forms of METTL3 determined by Edman
904 sequencing are shown.

905 FL indicates the full-length of METTL3. The short forms are labeled as a and b.

Figure 2

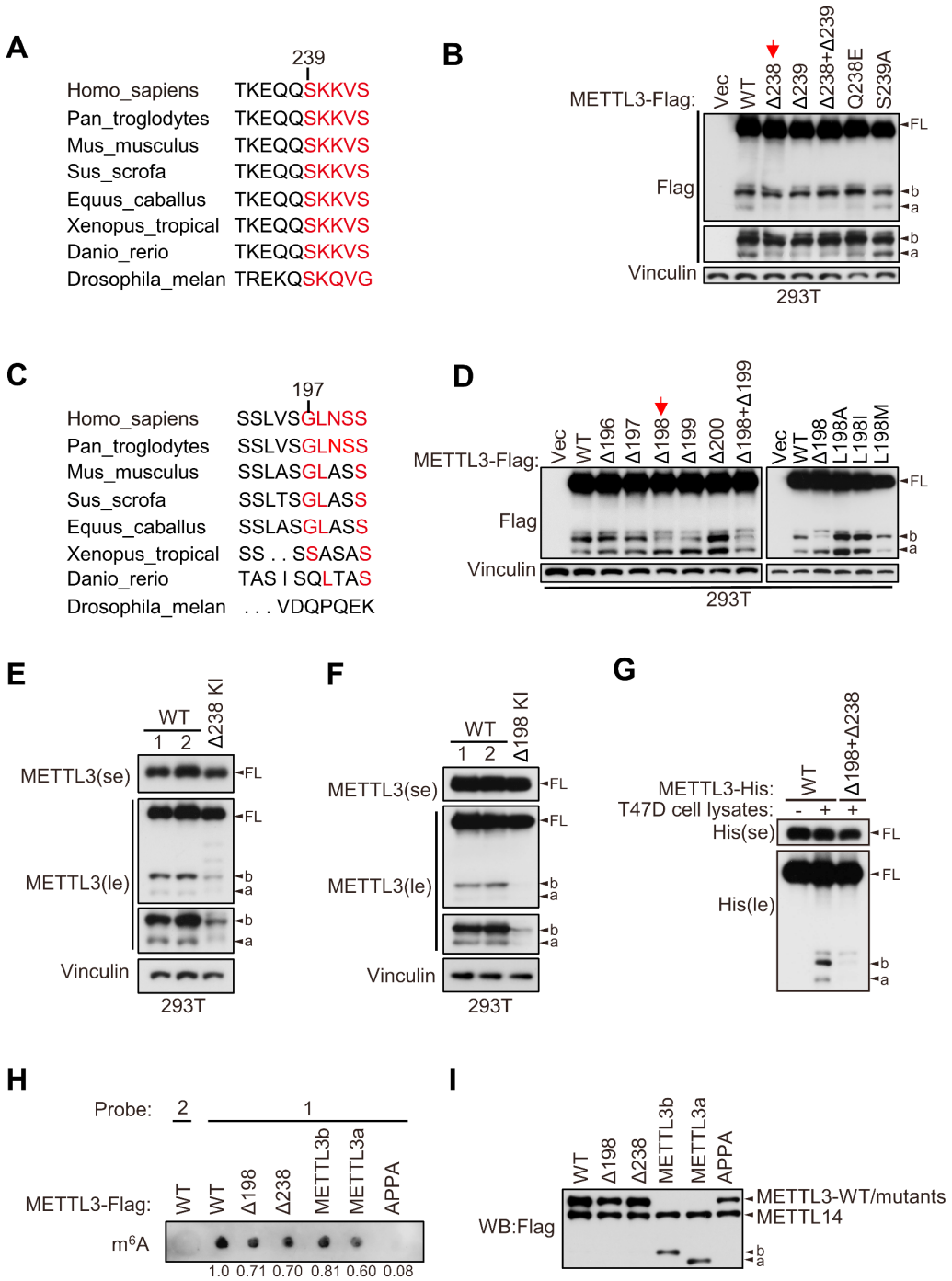

Figure 2. METTL3a (residues 239-580) and METTL3b (residues 197-580) are post-translational products through highly conserved residues

A and **C** Sequence alignments of the conserved residues on (234-244) (**A**) and (192-201) (**C**) of METTL3.

B and **D** Immunoblot of 293T cells transfected with empty vector (Vec) or METTL3-WT (wild type) or the indicated mutants.

E-F Immunoblot analysis of 293T cells with CRISPR knock-in (KI) mediated deletion of Q238 (**E**) or L198 (**F**).

G Purified recombinant METTL3-WT-His or METTL3-(Δ198+Δ238)-His protein were incubated with

or without T47D cell lysates at 37 °C for 1 h followed by immunoblot with anti-His antibody.

H-I The *in vitro* protein methylation activity was tested using purified METTL3-WT-Flag and its mutant proteins in combination with purified Flag-METTL14 and RNA-probe. The methylation of RNA-probe was measured by dot blot with the m^6A antibody (**H**), and the immunoblot of those purified proteins were shown in (**I**).

FL indicates the full-length of METTL3. The short forms are labeled as a and b. se and le indicated short exposure and long exposure, respectively.

Figure 3

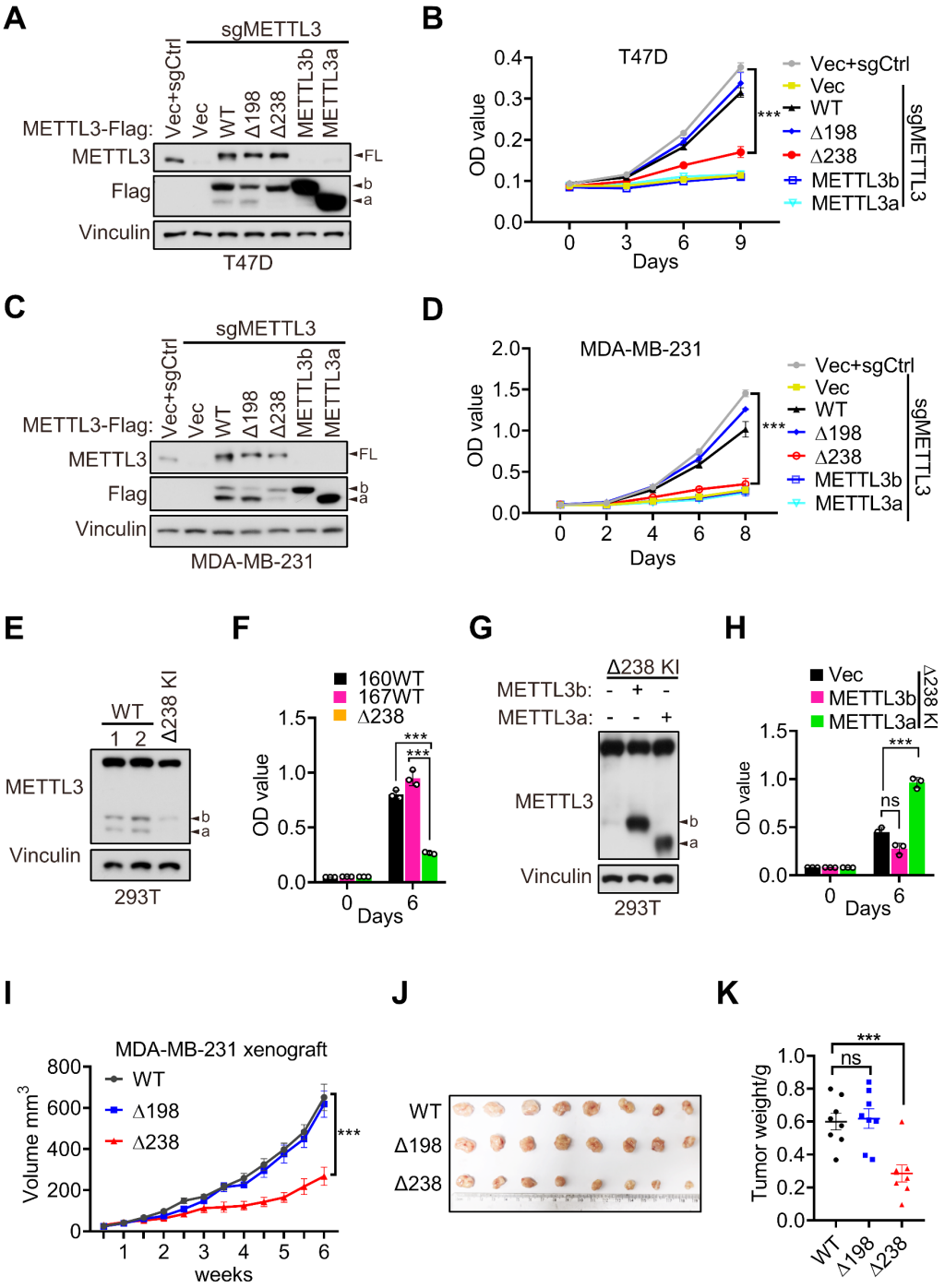

Figure 3. METTL3a contributes to cell proliferation and breast cancer progression

A-B Immunoblot (**A**) and cell proliferation (**B**) of T47D cells infected with retrovirus encoding sgMETTL3 resistant METTL3 variants or control vector (Vec) followed by another infection with sgMETTL3 or sgControl (sgCtrl).

C-D Immunoblot (**C**) and cell proliferation (**D**) of MDA-MB-231 cells infected with retrovirus encoding sgMETTL3 resistant METTL3 variants or control vector (Vec) followed by another infection with sgMETTL3 or sgControl (sgCtrl).

E-F Immunoblot (**E**) and cell proliferation (**F**) of 293T cells with WT or CRISPR knock-in mediated

deletion of Q238.

G-H Immunoblot analysis (**G**) cell proliferation (**H**) of Δ238 knock-in 293T cells rescued with METTL3a or METTL3b.

I-K Mouse xenograft experiments were performed with MDA-MB-231 cells infected with retrovirus encoding sgMETTL3 resistant METTL3-WT, METTL3-Δ198 or METTL3-Δ238 followed by another infection with sgMETTL3 (n=8 mice per group). Tumor growth curve (**I**), tumor (**J**) and tumor weight (**K**) were recorded. Error bars represent mean ± SEM, unpaired *t*-test. *** $P < 0.001$, ns denotes no significance. FL indicates the full-length of METTL3. The short forms are labeled as a and b.

Figure 4

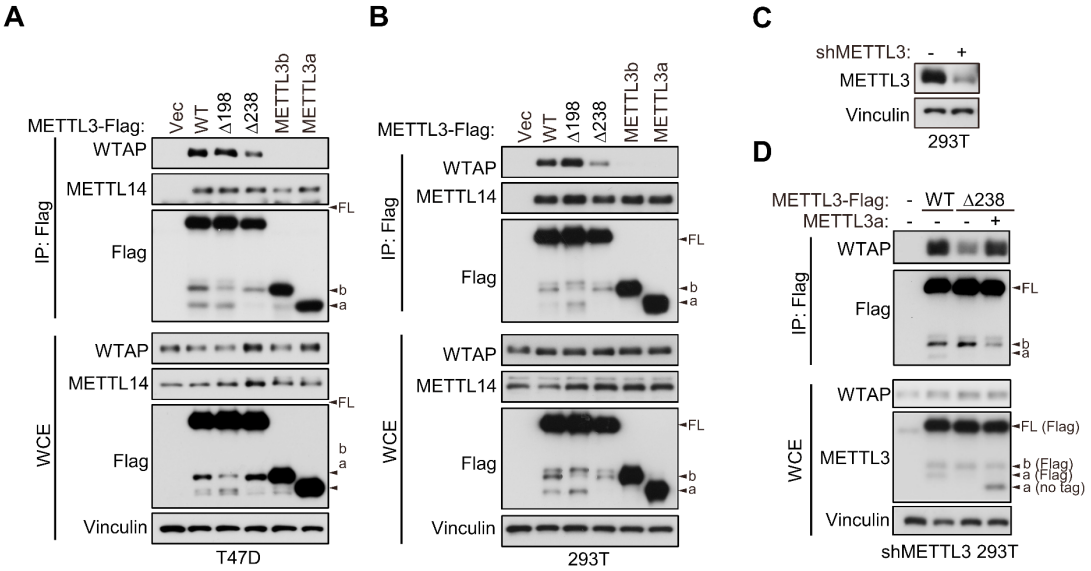

Figure 4. METTL3a is required for METTL3-WTAP interaction

A-B Co-immunoprecipitation analyses of T47D cells (**A**) and 293T cells (**B**) transfected with Vector (Vec), METTL3-WT or its mutants.

C Immunoblot analysis of 293T cells infected with or without lentivirus encoding METLL3 shRNA.

D Immunoblot of whole cell extracts (WCE) and immunoprecipitations (IP) of 293T cells infected with lentivirus encoding METLL3 shRNA followed by transfection with METTL3-WT-Flag, METTL3-Δ238-Flag combining with or without METTL3a (no flag tag), or control vector as indicated.

Figure 5

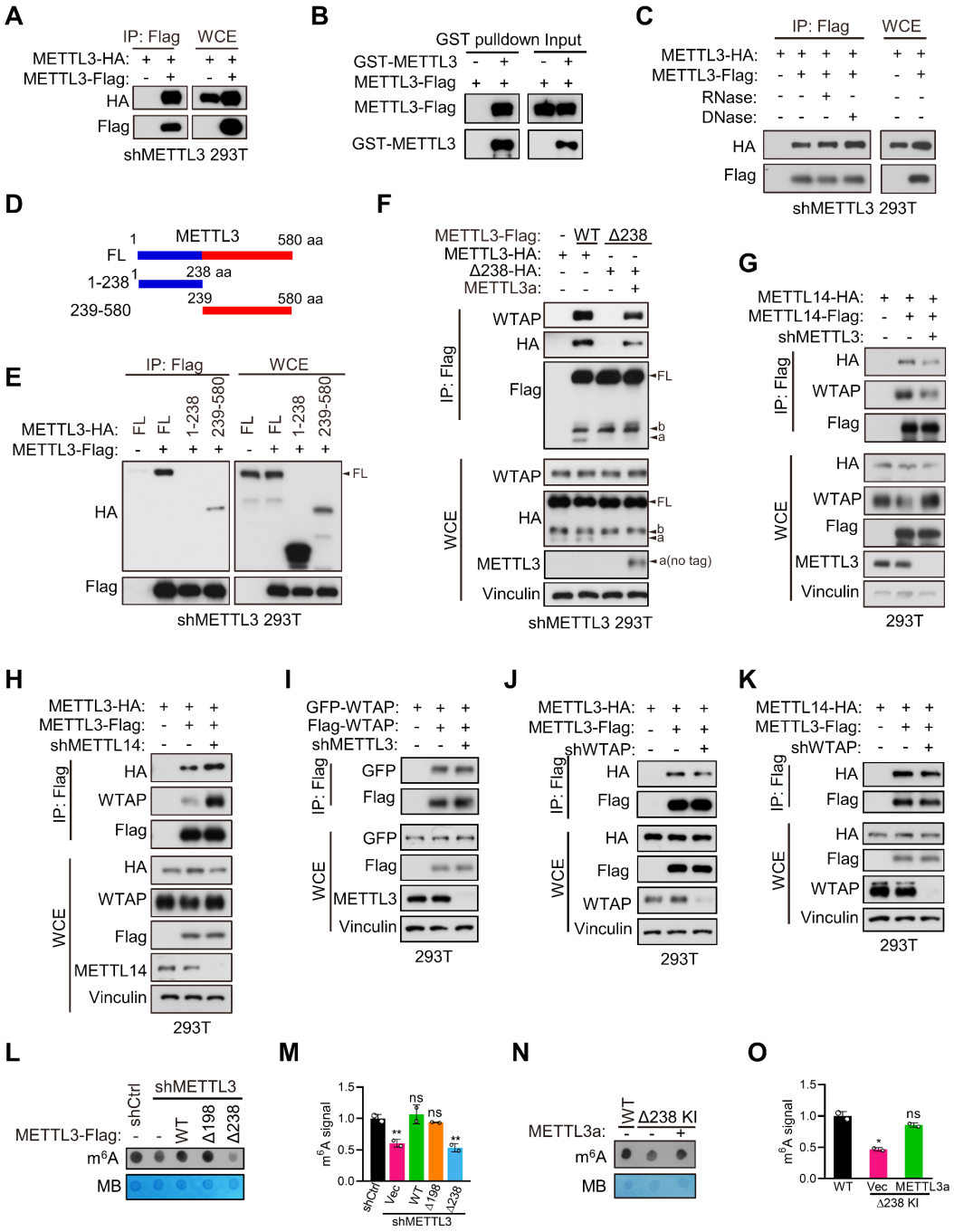

Figure 5. METTL3a mediates the METTL3-METTL3 interaction, a prerequisite step for WTAP recruitment in MTC complex

A Immunoblot of whole cell extracts (WCE) and immunoprecipitations (IP) of 293T transfected with METTL3 containing different tag.

B Immunoblot analysis showing the binding between purified METTL3-Flag and GST-METTL3.

C Immunoblot of whole cell extracts (WCE) and immunoprecipitations (IP) of 293T transfected with METTL3 containing different tag with or without RNase or DNase.

D A schematic representation of METTL3 and its truncations used for immunoprecipitation.

E Immunoblot of whole cell extracts (WCE) and immunoprecipitations (IP) of 293T cells infected with

lentivirus encoding METLL3 shRNA followed by transfection with full-length (FL) or truncation of METTL3.

F Immunoblot of whole cell extracts (WCE) and immunoprecipitations (IP) of 293T cells infected with lentivirus encoding METLL3 shRNA followed by transfection with METTL3-WT-flag, METTL3-Δ238-Flag combining with or without METTL3a (no flag tag) or control vector as indicated.

G-H Immunoblot of whole cell extracts (WCE) and immunoprecipitations (IP) of 293T cells infected with or without lentivirus encoding METLL3 shRNA (**G**) or METTL14 shRNA (**H**) followed by transfection with METTL3 or METTL14 as indicated.

I Immunoblot of whole cell extracts (WCE) and immunoprecipitations (IP) of 293T cells infected with lentivirus encoding METTL3 shRNA followed by transfection with WTAP containing different tag.

J- K Immunoblot of whole cell extracts (WCE) and immunoprecipitations (IP) of 293T cells infected with lentivirus encoding WTAP shRNA followed by transfection with METTL3 or METTL14 as indicated.

L-M m^6A dot blot (**L**) and quantification (**M**) of 293T cells infected with lentivirus encoding METLL3 shRNA followed by transfection with METTL3-WT, METTL3 variants, or control vector as indicated. Methylene blue (MB) is used as a loading control.

N-O m^6A dot blot (**N**) and quantification (**O**) of 293T cells with WT or CRISPR knock-in mediated deletion of Q238 with or without transfection of METTL3a.

FL indicates the full-length of METTL3. The short forms are labeled as a and b. no tag represents exogenous METTL3a containing no flag tag.

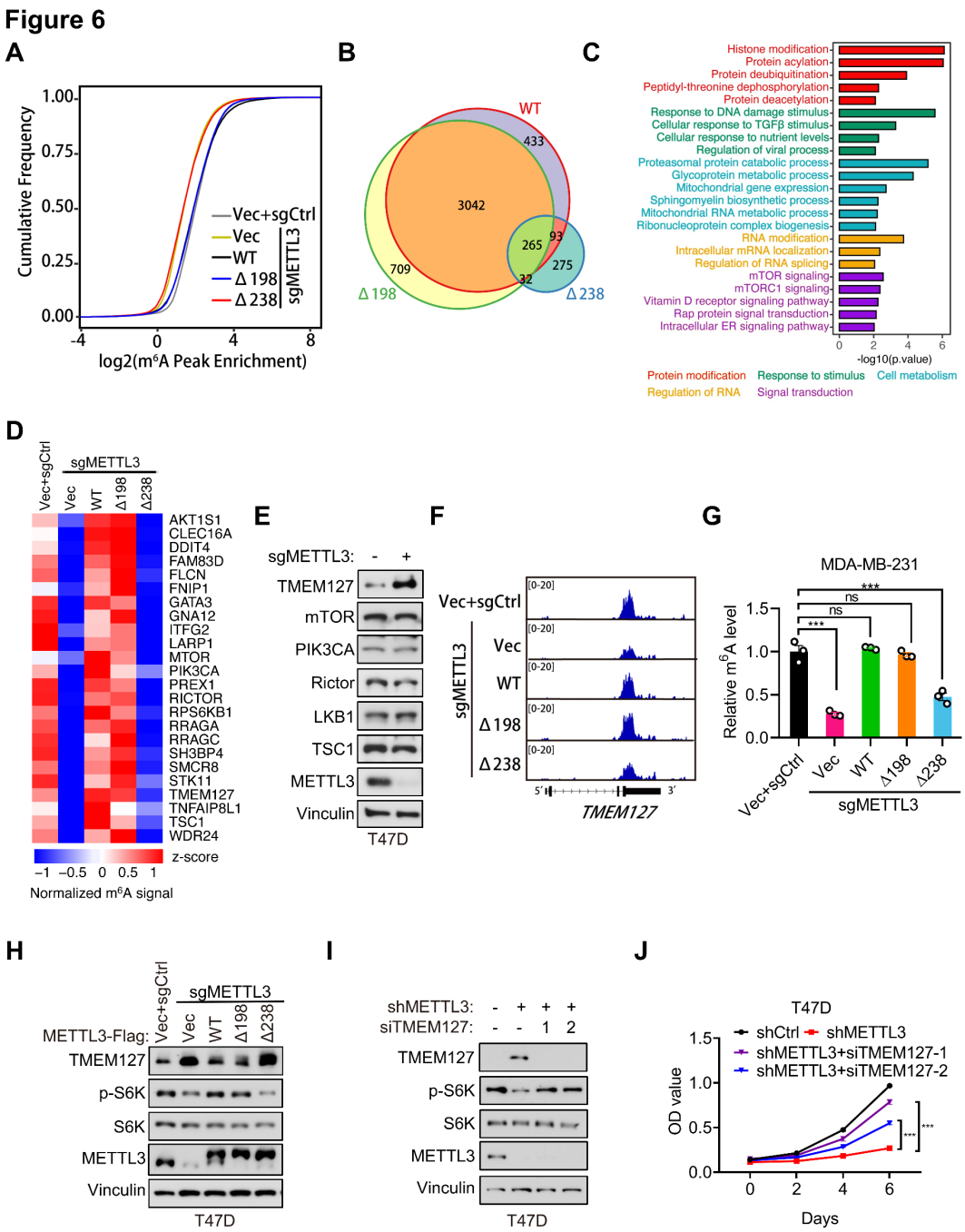

1028

1029 **Figure 6. METTL3a is essential for the global METTL3-mediated m^{6}A deposition and mTOR**
1030 **activation**

1031 **A** Cumulative distribution function of log2 peak intensity of m^{6}A-modified sites in T47D cells infected
1032 with retrovirus encoding sgMETTL3 resistant METTL3-WT, METTL3-Δ198, METTL3-Δ238 or control
1033 vector (Vec) followed by another infection with sgMETTL3 or sgControl (sgCtrl).

1034 **B** Overlaps of m^{6}A peaks among METTL3-WT, METTL3-Δ198 and METTL3-Δ238 in METTL3 KO
1035 T47D cells.

1036 **C** GSEA with GO terms of differentially m^{6}A methylated peaks in METTL3-WT and METTL3-Δ238
1037 for molecular functions.

1038 **D** Heat map of m^{6}A peaks related to mTOR pathway in T47D cells infected with retrovirus encoding

sgMETTL3 resistant METTL3-WT, METTL3-Δ198, METTL3-Δ238 or control vector (Vec) followed by another infection with sgMETTL3 or sgControl (sgCtrl).

E Immunoblot analysis of T47D cells infected with sgControl or sgMETTL3.

F Integrative genomic viewer (IGV) plots of m^6A peaks at *TMEM127* mRNA in T47D cells as described in (**A**).

G m^6A-qPCR showing the m^6A enriched *TMEM127* transcripts from T47D cells.

H Immunoblot of cell lysates from T47D cells as described in (**A**).

I-J Immunoblot (**I**) and cell proliferation (**J**) of T47D cells infected with shMETTL3 or shControl followed by transfection with siTMEM127 or siControl.

Error bars represent mean ± SEM, unpaired *t*-test. *** $P < 0.001$, ns denotes no significance.

Figure 7

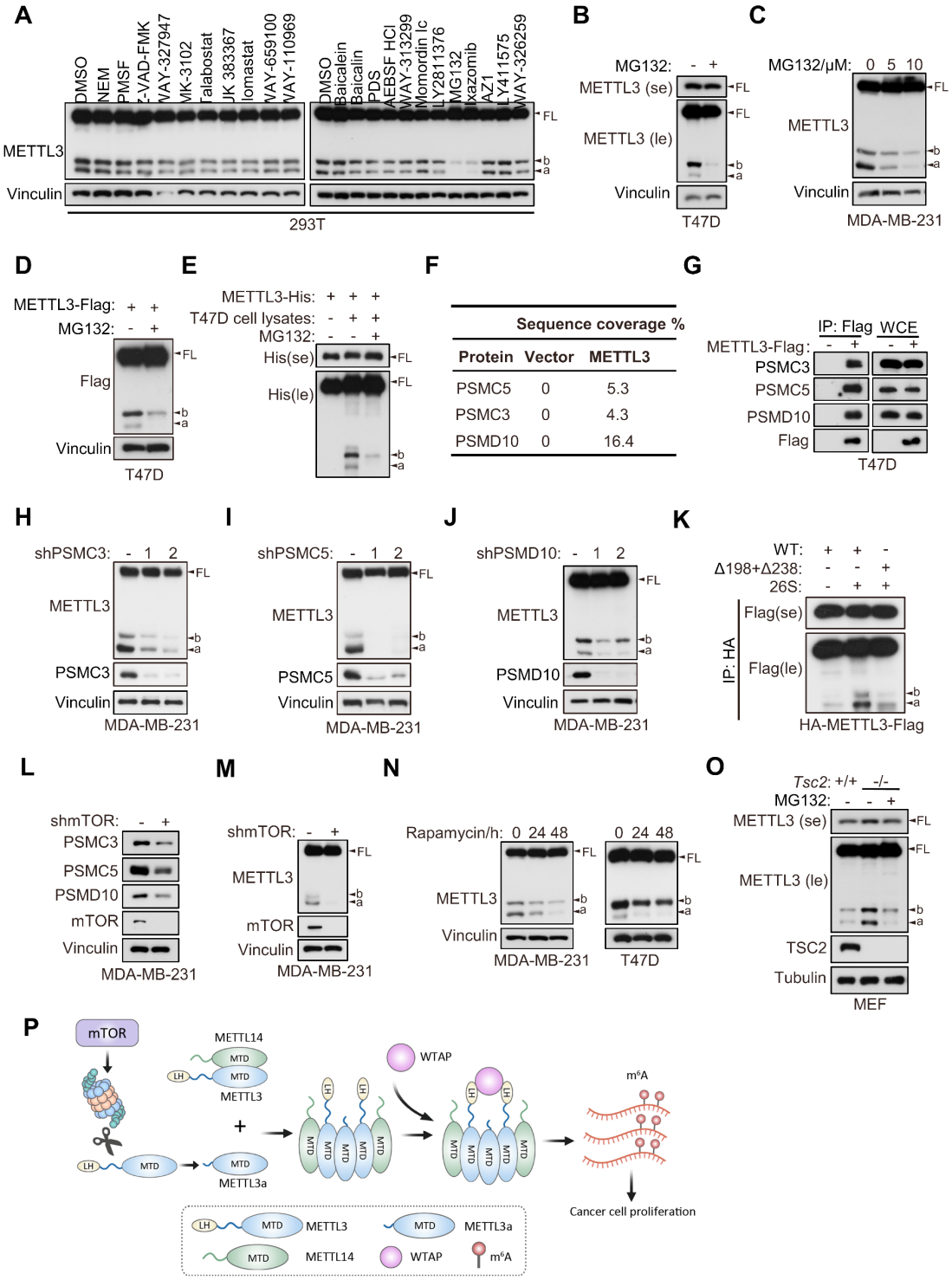

Figure 7. Proteasome mediates METTL3 cleavage in an mTOR-dependent manner

A Immunoblot of T47D cells treated with indicated inhibitors.

B-C Immunoblot of T47D (**B**) and MDA-MB-231 (**C**) cells treated with MG132 for 8 hours.

D Immunoblot of T47D cells infected with METTL3-Flag followed by treatment with MG132 (10 μM) for 8 h.

E Immunoblot of purified recombinant METTL3-His protein incubated with or without T47D cell lysates

wherein with or without MG132 treatment (20 μM) at 37 °C for 1 h.

F List of the proteasome components identified by LC-MS/MS analysis of the tandem affinity purification with METTL3 antibody in 293T cells.

G Immunoblot of whole cell extracts (WCE) and immunoprecipitations (IP) of T47D cells infected with METTL3-Flag or control vector.

H-J Immunoblot of MDA-MB-231 cells infected with shControl, shPSMC3 (**H**), shPSMC5 (**I**), shPSMD10 (**J**).

K Immunoblot of the purified HA-METTL3-Flag WT or indicated mutant from 293T cells using HA-magnetic beads followed by incubation with 26S at 37 °C for 1 h.

L-M Immunoblot of MDA-MB-231 cells infected with shmTOR or shControl.

N Immunoblot of T47D cells or MDA-MB-231 cells with time course treatment of rapamycin (100 nM) as indicated.

O Immunoblot of *Tsc2* WT (*Tsc2*$^{+/+}$) or *Tsc2* KO (*Tsc2*$^{-/-}$) MEF cells treated with or without MG132 (10 μM) for 8 h.

P A model for METTL3a-mediated MTC complex assembly.

FL indicates the full-length of METTL3. The short forms are labeled as a and b. se and le indicated short exposure and long exposure, respectively.

1090 **Supplementary Figures**

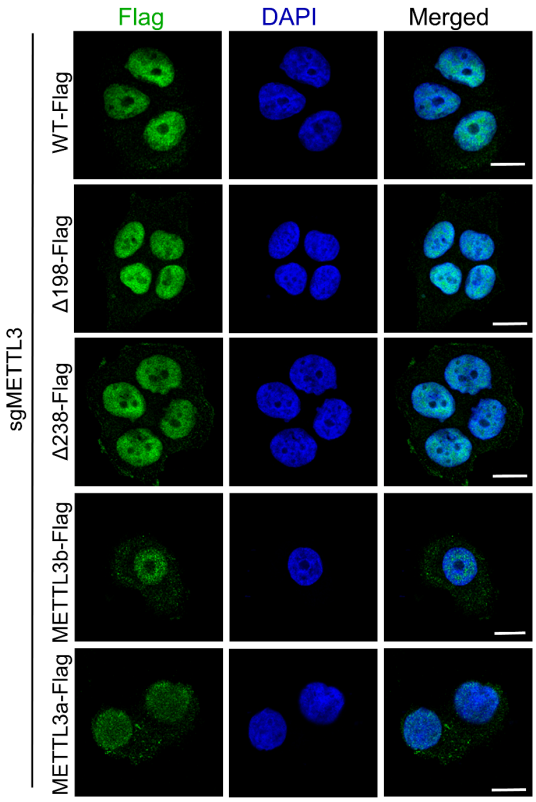

1091 **Supplementary Figure 1. Distribution of METTL3-WT and its mutants in breast cancer cells.**

1092 Immunofluorescence analysis of T47D cells stably expressing METTL3-WT or mutants under METTL3
1093 knockout. Scale bars, 10 μm.
1094
1095
1096
1097
1098
1099
1100
1101
1102

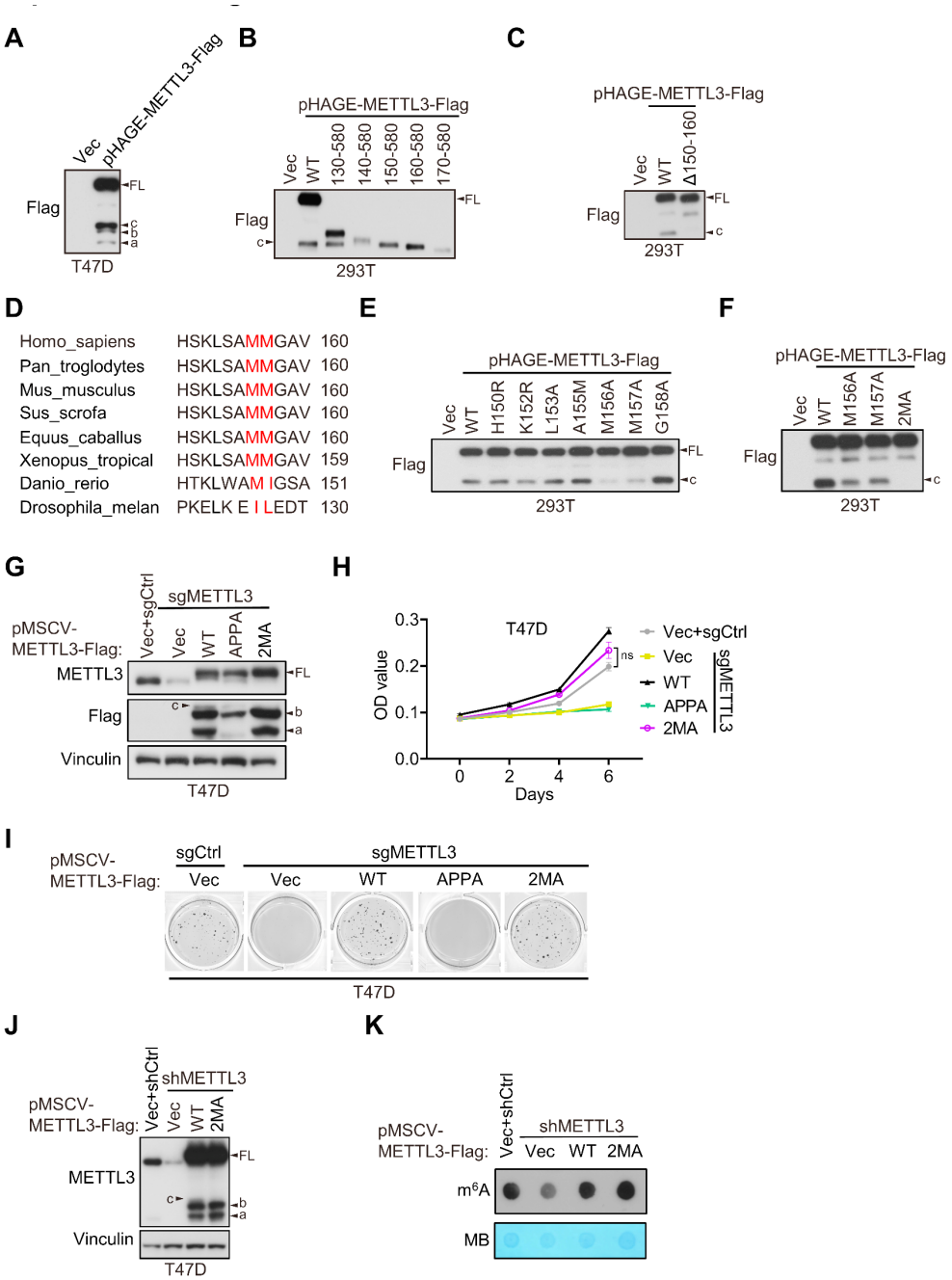

Supplementary Figure 2. The short form METTL3c is dispensable for METTL3-mediated functions.

A Immunoblot of T47D cells infected with pHAGE-METTL3-Flag. **B-C**, **E-F** Immunoblot of 293T cells transfected with pHAGE-METTL3-WT or its indicated mutants. **D** Sequence alignment of conserved amino acids on (150-160) of METTL3. **G-I** Immunoblot analysis (**G**), cell proliferation (**H**) and soft agar growth (**i**) of T47D cells infected with retrovirus encoding Vector (Vec), sgMETTL3 resistant METTL3-WT or its indicated mutants followed by another infection with sgMETTL3 or sgControl (sgCtrl). **J-K** Immunoblot analysis (**J**) and m^6A dot blot (**K**) in 293T cells infected with shMETTL3 or shControl (shCtrl) followed by transfection with indicated plasmids. Methylene blue (MB) was used as a loading control. Error bars represent mean ± SEM, unpaired *t*-test. ns denotes not significant. FL is the full-length of METTL3. The short forms are labeled a, b and c.

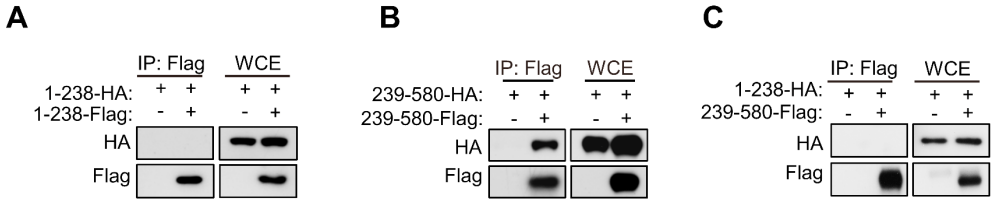

Supplementary Figure 3. The METTL3-METTL3 interaction depends on its C-terminal region. **A-C** Immunoblot of whole cell extracts (WCE) and immunoprecipitations (IP) of 293T cells infected with lentivirus encoding METLL3 shRNA followed by transfection with the truncation of METTL3 as indicated.

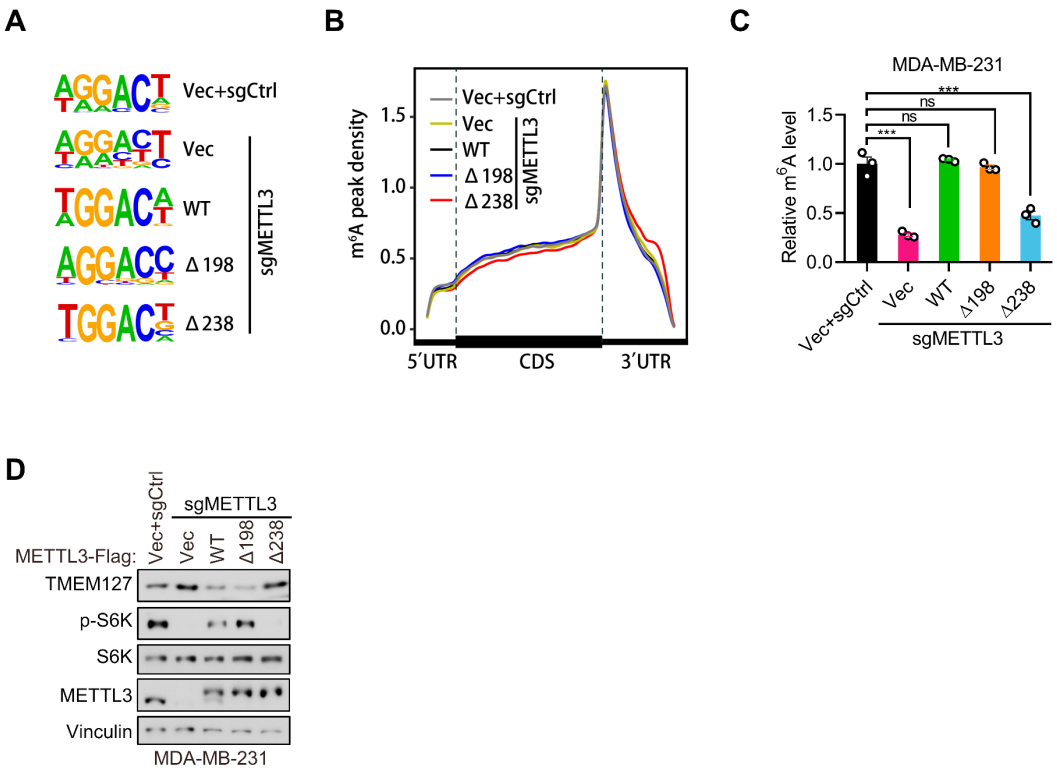

Supplementary Figure 4. METTL3a is essential for the global METTL3-mediated m^{6}A deposition and mTOR activation

A-B Consensus motifs (**A**), and the distribution (**B**) of m^{6}A-modified sites in T47D cells infected with retrovirus encoding sgMETTL3 resistant METTL3-WT, METTL3-Δ198, METTL3-Δ238 or control vector (Vec) followed by another infection with sgMETTL3 or sgControl (sgCtrl). **C** RIP-qPCR showing the m^{6}A enriched *TMEM127* transcripts from MD-MB-231 cells infected with retrovirus encoding sgMETTL3 resistant METTL3-WT, METTL3-Δ198, METTL3-Δ238 or control vector (Vec) followed by another infection with sgMETTL3 or sgControl (sgCtrl). **D** Immunoblot of cell lysates from T47D cells as described in (**C**). Error bars represent mean ± SEM, unpaired *t*-test. *** $P < 0.001$, ns denotes no significance.

A

cat. Number	Name	Target
S3692	N-Ethylmaleimide (NEM)	Cysteine Protease
S3025	PMSF	irreversible serine/cysteine protease
S8102	Z-VAD(OH)-FMK	irreversible pan-caspase inhibitor
P2550	WAY-327947	caspase
S8565	Omarigliptin (MK-3102)	DPP-4
S8455	Talabostat (Val-boroPro, PT-100)	dipeptidyl peptidase
S2224	UK 383367	Procollagen C Proteinase
S7157	Ilomastat (GM6001, Galardin)	MMP
P3183	WAY-659100	hormone sensitive lipase (HSL); metalloprotease
P2039	WAY-110969	tyrosinase
S2268	Baicalein	P450 (e.g. CYP17), endopeptidase
S2269	Baicalin	GABA Receptor, endopeptidase
S7382	Phosphoramidon Disodium Salt (PDS)	endopeptidase
S7378	AEBSF HCl	Serine Protease
P2246	WAY-313299	JAMM protease
S9159	Momordin Ic	SENP1
S1528	LY2811376	non-peptidic β-secretase(BACE1)
S2619	MG-132	proteasome and calpain
S2180	Ixazomib (MLN2238)	20S proteasome
S8904	AZ1	ubiquitin-specific protease (USP) 25/28.
S2714	LY411575	γ-secretase
P2462	WAY-326259	thrombin; factor XIa

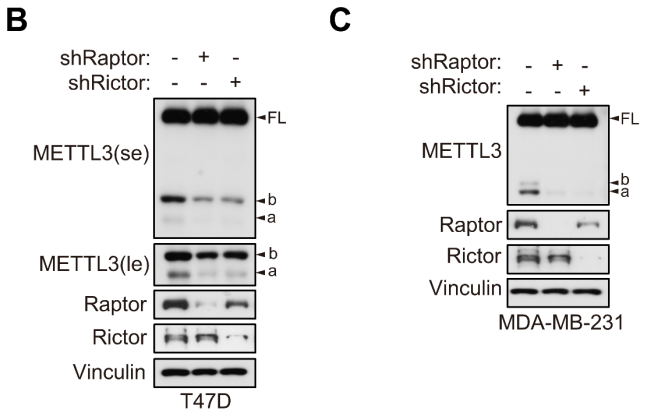

Supplementary Figure 5. Proteasome mediates METTL3 cleavage in an mTOR-dependent manner
A Information on protease inhibitors utilized in Figure 7**A**. **B-C** Immunoblot analyses of T47D cells (**B**) or MDA-MB-231(**C**) cells infected with shControl, shRaptor or shRictor.

Figure 1

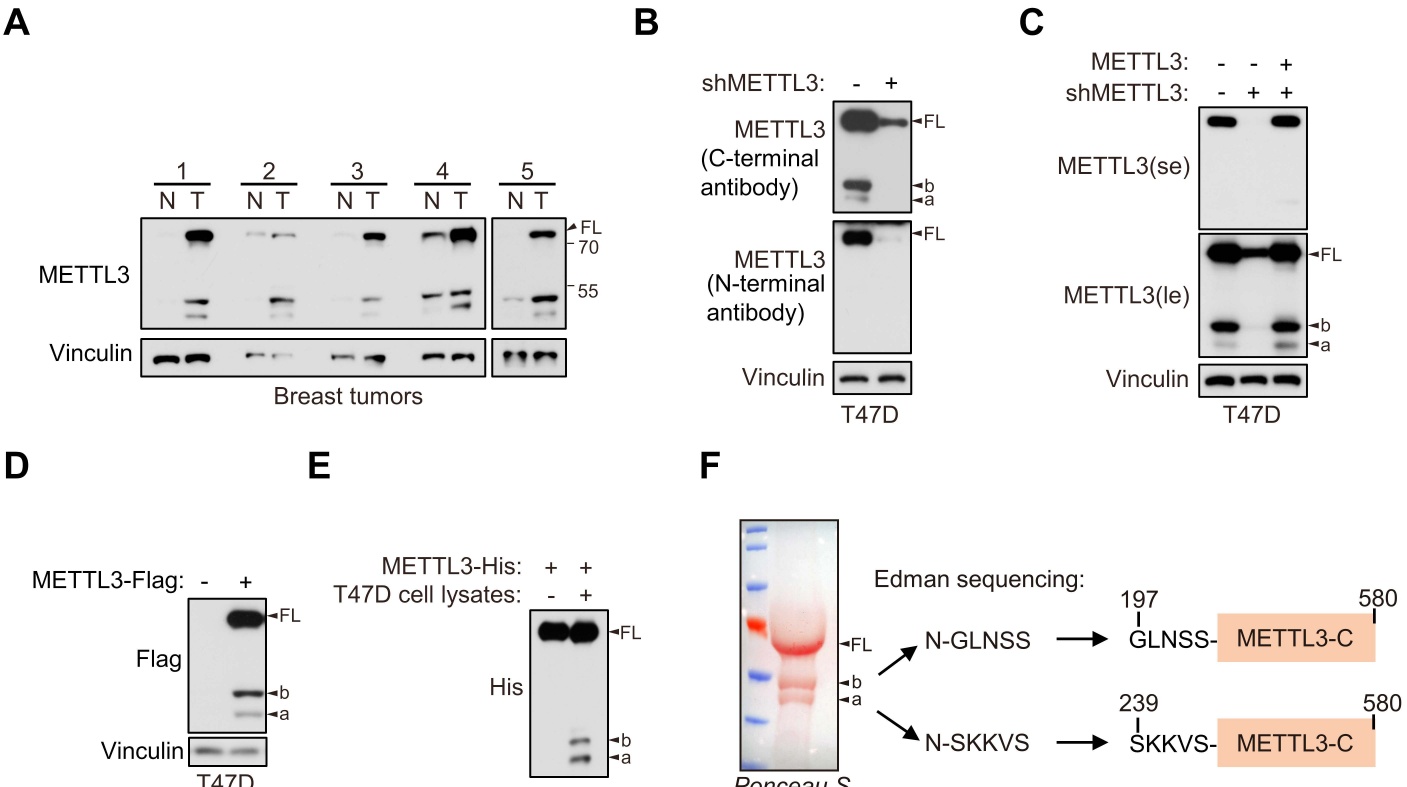
A
1
2
3
4
5
N T
N T
N T
N T
N T
METTL3
Vinculin
FL
70
55
Breast tumors
B
shMETTL3: - +
METTL3 (C-terminal antibody)
METTL3 (N-terminal antibody)
FL
b
a
Vinculin
T47D
C
METTL3: - - +
shMETTL3: - + +
METTL3(se)
METTL3(le)
FL
b
a
Vinculin
T47D
D
METTL3-Flag: - +
Flag
FL
b
a
Vinculin
T47D
E
METTL3-His: + +
T47D cell lysates: - +
His
FL
b
a
F
FL
b
a
Ponceau S
Edman sequencing:
N-GLNSS
197
GLNSS-
METTL3-C
580
N-SKKVS
239
SKKVS-
METTL3-C
580

Figure 2

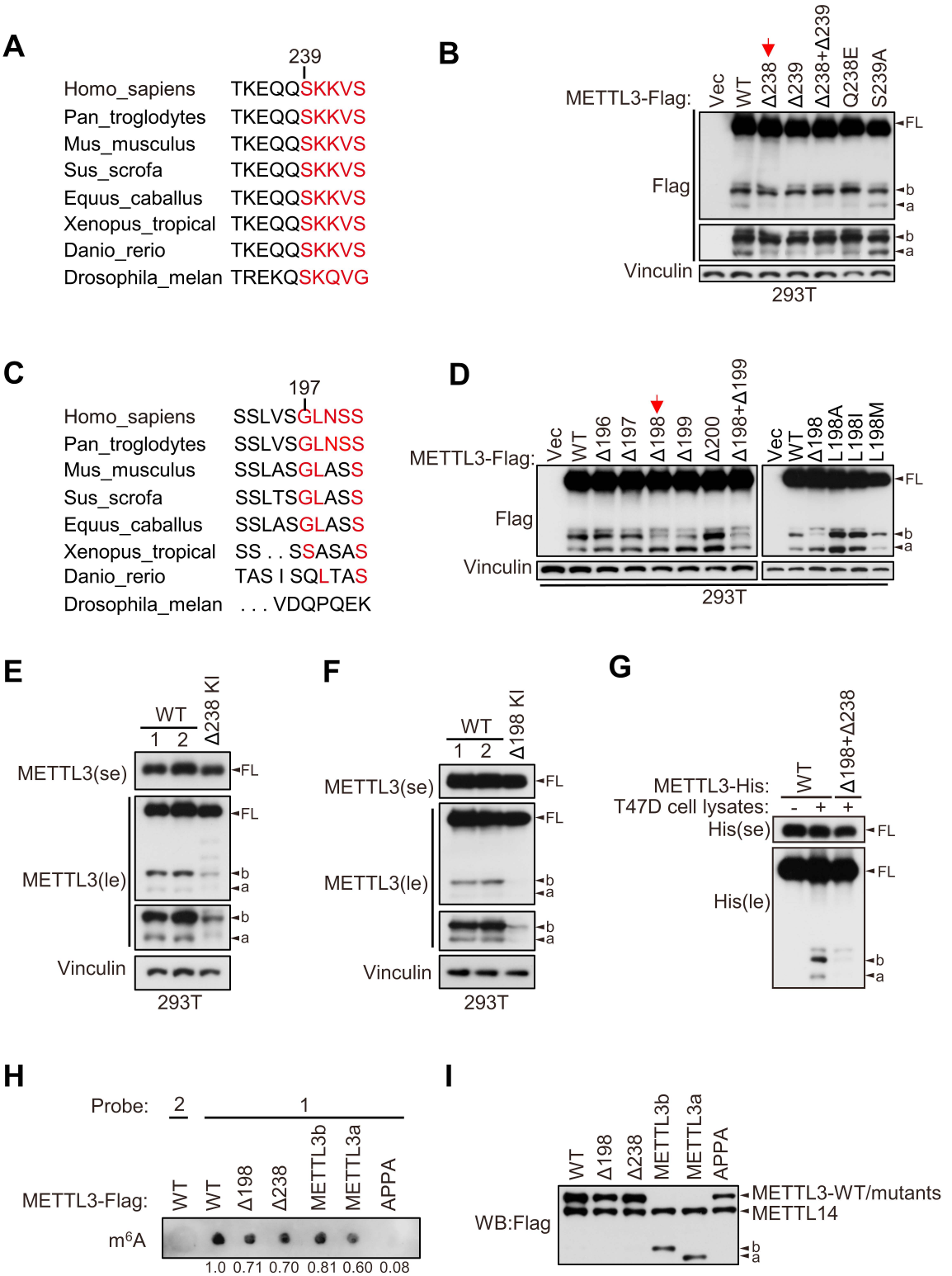
A
239
Homo_sapiens TKEQQSKKVS
Pan_troglodytes TKEQQSKKVS
Mus_musculus TKEQQSKKVS
Sus_scrofa TKEQQSKKVS
Equus_caballus TKEQQSKKVS
Xenopus_tropical TKEQQSKKVS
Danio_rerio TKEQQSKKVS
Drosophila_melan TREKQSKQVG
B
METTL3-Flag:
Vec
WT
Δ238
Δ239
Δ238+Δ239
Q238E
S239A
Flag
Vinculin
FL
b
a
293T
C
197
Homo_sapiens SSLVSGLNSS
Pan_troglodytes SSLVSGLNSS
Mus_musculus SSLASGLASS
Sus_scrofa SSLTSGLASS
Equus_caballus SSLASGLASS
Xenopus_tropical SS . . SSASAS
Danio_rerio TAS I SQLTAS
Drosophila_melan . . . VDQPQEK
D
METTL3-Flag:
Vec
WT
Δ196
Δ197
Δ198
Δ199
Δ200
Δ198+Δ199
Vec
WT
Δ198
L198A
L198I
L198M
Flag
Vinculin
FL
b
a
293T
E
WT
1 2
Δ238 KI
METTL3(se)
METTL3(le)
Vinculin
FL
b
a
293T
F
WT
1 2
Δ198 KI
METTL3(se)
METTL3(le)
Vinculin
FL
b
a
293T
G
METTL3-His:
T47D cell lysates:
WT
Δ198+Δ238
- + +
His(se)
His(le)
FL
b
a
H
Probe: 2 1
METTL3-Flag:
WT
WT
Δ198
Δ238
METTL3b
METTL3a
APPA
m6A
1.0 0.71 0.70 0.81 0.60 0.08
I
WT
Δ198
Δ238
METTL3b
METTL3a
APPA
WB:Flag
METTL3-WT/mutants
METTL14
b
a

Figure 3

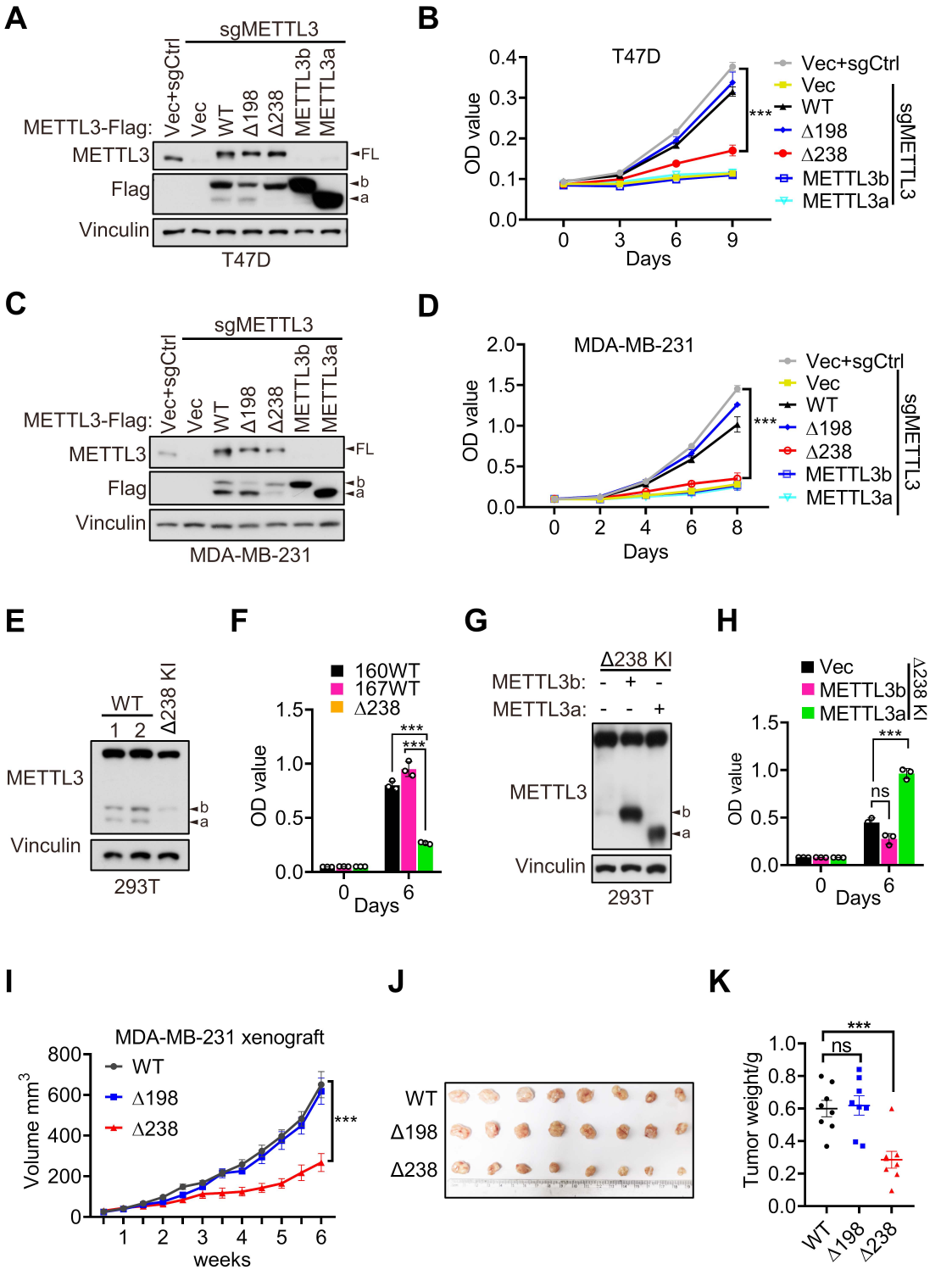
A
sgMETTL3
Vec+sgCtrl
Vec
WT
Δ198
Δ238
METTL3b
METTL3a
METTL3-Flag:
METTL3
Flag
Vinculin
FL
b
a
T47D
B
T47D
OD value
Days
Vec+sgCtrl
Vec
WT
Δ198
Δ238
METTL3b
METTL3a
sgMETTL3
***
C
sgMETTL3
METTL3-Flag:
METTL3
Flag
Vinculin
MDA-MB-231
D
MDA-MB-231
OD value
Days
E
WT
1 2
Δ238 KI
METTL3
Vinculin
293T
F
160WT
167WT
Δ238
OD value
Days
***
G
Δ238 KI
METTL3b:
METTL3a:
METTL3
Vinculin
293T
H
Vec
METTL3b
METTL3a
Δ238 KI
OD value
Days
ns
***
I
MDA-MB-231 xenograft
WT
Δ198
Δ238
Volume mm3
weeks
***
J
WT
Δ198
Δ238
K
Tumor weight/g
ns
***
WT
Δ198
Δ238

Figure 4

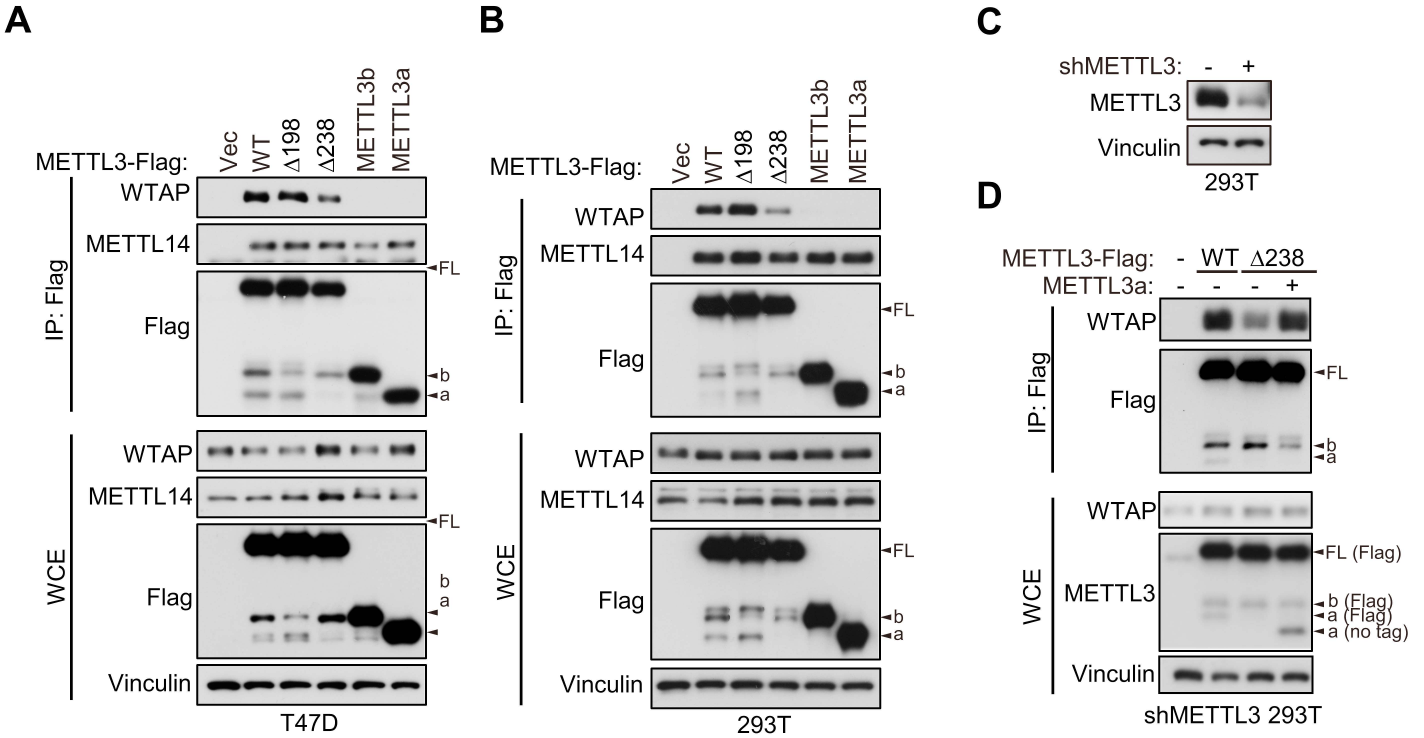
A
METTL3-Flag:
Vec
WT
Δ198
Δ238
METTL3b
METTL3a
IP: Flag
WTAP
METTL14
Flag
FL
b
a
WCE
WTAP
METTL14
Flag
FL
b
a
Vinculin
T47D
B
METTL3-Flag:
Vec
WT
Δ198
Δ238
METTL3b
METTL3a
IP: Flag
WTAP
METTL14
Flag
FL
b
a
WCE
WTAP
METTL14
Flag
FL
b
a
Vinculin
293T
C
shMETTL3: - +
METTL3
Vinculin
293T
D
METTL3-Flag: - WT Δ238
METTL3a: - - - +
IP: Flag
WTAP
Flag
FL
b
a
WCE
WTAP
METTL3
FL (Flag)
b (Flag)
a (Flag)
a (no tag)
Vinculin
shMETTL3 293T

Figure 5

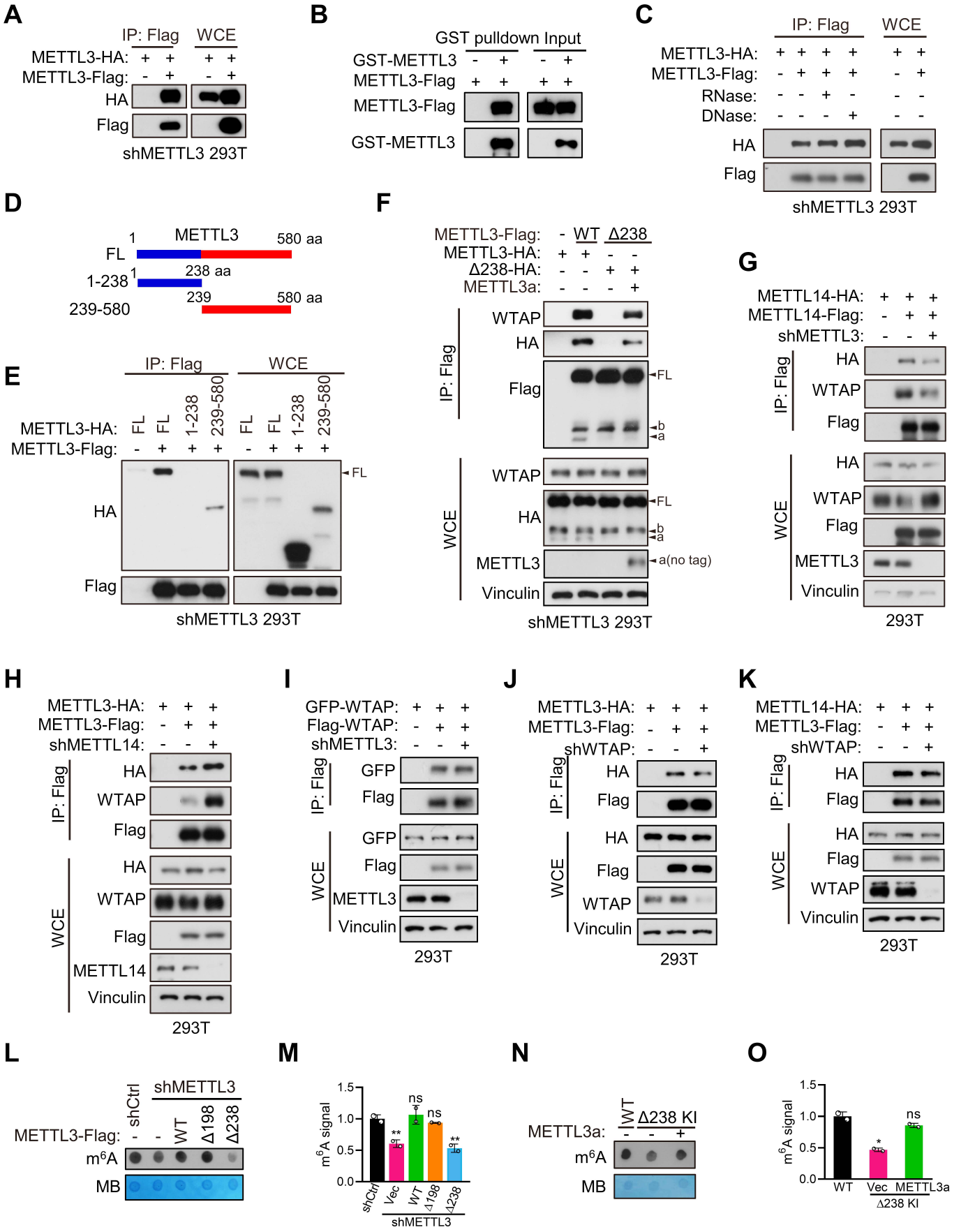
A
IP: Flag
WCE
METTL3-HA:
METTL3-Flag:
HA
Flag
shMETTL3 293T
B
GST pulldown
Input
GST-METTL3
METTL3-Flag
GST-METTL3
C
IP: Flag
WCE
METTL3-HA:
METTL3-Flag:
RNase:
DNase:
HA
Flag
shMETTL3 293T
D
METTL3
FL
1-238
239-580
1
580 aa
238 aa
239
E
IP: Flag
WCE
METTL3-HA:
METTL3-Flag:
FL
1-238
239-580
HA
Flag
shMETTL3 293T
F
METTL3-Flag:
WT
Δ238
METTL3-HA:
Δ238-HA:
METTL3a:
IP: Flag
WCE
WTAP
HA
Flag
METTL3
Vinculin
a(no tag)
shMETTL3 293T
G
METTL14-HA:
METTL14-Flag:
shMETTL3:
IP: Flag
WCE
HA
WTAP
Flag
METTL3
Vinculin
293T
H
METTL3-HA:
METTL3-Flag:
shMETTL14:
IP: Flag
WCE
HA
WTAP
Flag
METTL14
Vinculin
293T
I
GFP-WTAP:
Flag-WTAP:
shMETTL3:
IP: Flag
WCE
GFP
Flag
METTL3
Vinculin
293T
J
METTL3-HA:
METTL3-Flag:
shWTAP:
IP: Flag
WCE
HA
Flag
WTAP
Vinculin
293T
K
METTL14-HA:
METTL3-Flag:
shWTAP:
IP: Flag
WCE
HA
Flag
WTAP
Vinculin
293T
L
shCtrl
shMETTL3
METTL3-Flag:
WT
Δ198
Δ238
m6A
MB
M
m6A signal
1.5
1.0
0.5
0.0
ns
ns
**
**
shCtrl
Vec
WT
Δ198
Δ238
shMETTL3
N
METTL3a:
WT
Δ238 KI
m6A
MB
O
m6A signal
1.5
1.0
0.5
0.0
ns
*
WT
Vec
METTL3a
Δ238 KI

Figure 6

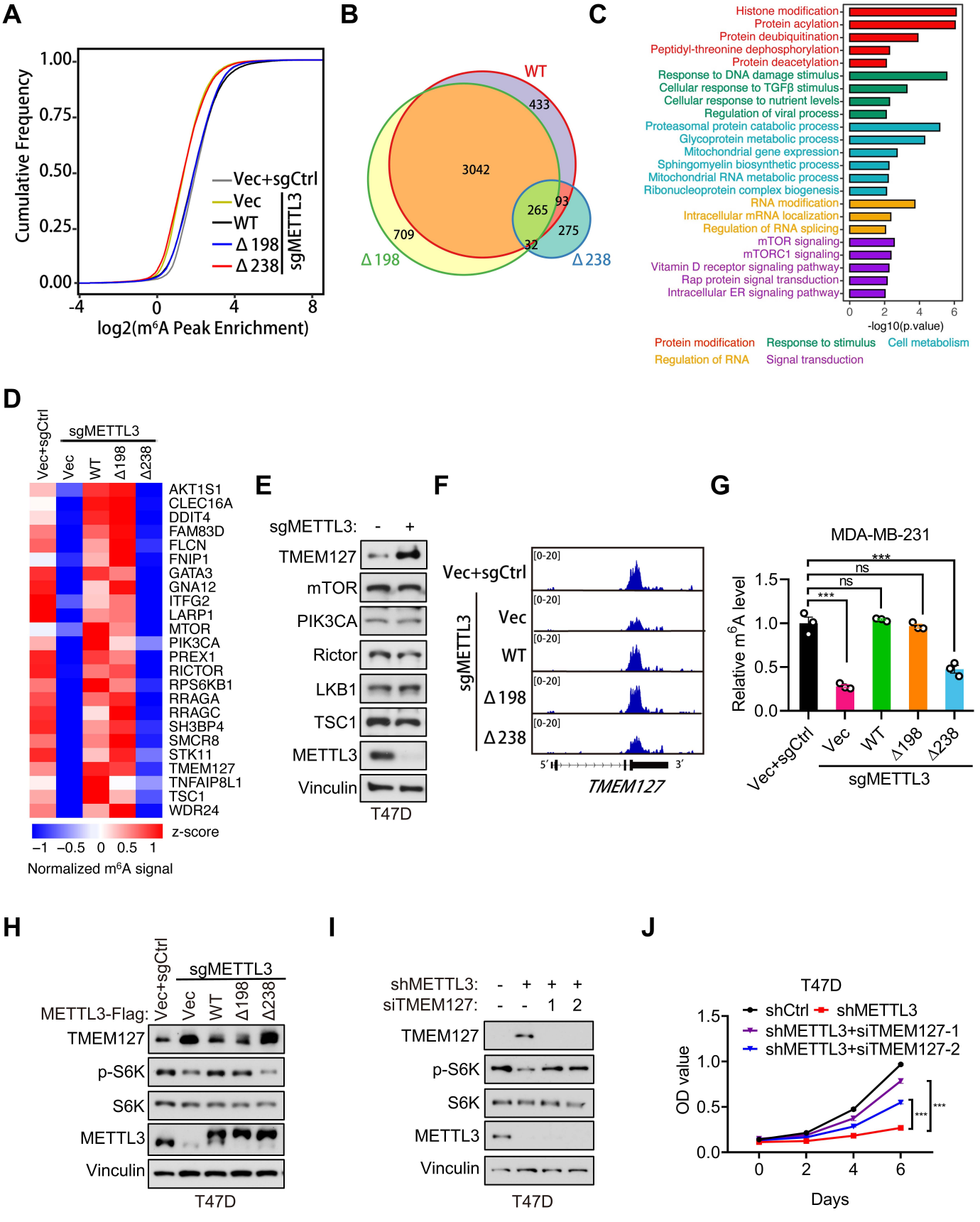
A
Cumulative Frequency
1.00
0.75
0.50
0.25
0.00
-4
0
4
8
log2(m6A Peak Enrichment)
Vec+sgCtrl
Vec
WT
Δ198
Δ238
sgMETTL3
B
WT
433
3042
709
265
93
275
32
Δ198
Δ238
C
Histone modification
Protein acylation
Protein deubiquitination
Peptidyl-threonine dephosphorylation
Protein deacetylation
Response to DNA damage stimulus
Cellular response to TGFβ stimulus
Cellular response to nutrient levels
Regulation of viral process
Proteasomal protein catabolic process
Glycoprotein metabolic process
Mitochondrial gene expression
Sphingomyelin biosynthetic process
Mitochondrial RNA metabolic process
Ribonucleoprotein complex biogenesis
RNA modification
Intracellular mRNA localization
Regulation of RNA splicing
mTOR signaling
mTORC1 signaling
Vitamin D receptor signaling pathway
Rap protein signal transduction
Intracellular ER signaling pathway
0
2
4
6
-log10(p.value)
Protein modification
Response to stimulus
Cell metabolism
Regulation of RNA
Signal transduction
D
Vec+sgCtrl
sgMETTL3
Vec
WT
Δ198
Δ238
AKT1S1
CLEC16A
DDIT4
FAM83D
FLCN
FNIP1
GATA3
GNA12
ITFG2
LARP1
MTOR
PIK3CA
PREX1
RICTOR
RPS6KB1
RRAGA
RRAGC
SH3BP4
SMCR8
STK11
TMEM127
TNFAIP8L1
TSC1
WDR24
z-score
−1 −0.5 0 0.5 1
Normalized m6A signal
E
sgMETTL3: - +
TMEM127
mTOR
PIK3CA
Rictor
LKB1
TSC1
METTL3
Vinculin
T47D
F
Vec+sgCtrl
sgMETTL3
Vec
WT
Δ198
Δ238
[0-20]
5′
3′
TMEM127
G
MDA-MB-231
Relative m6A level
1.5
1.0
0.5
0.0
***
ns
ns
***
Vec+sgCtrl
Vec
WT
Δ198
Δ238
sgMETTL3
H
Vec+sgCtrl
sgMETTL3
METTL3-Flag:
Vec
WT
Δ198
Δ238
TMEM127
p-S6K
S6K
METTL3
Vinculin
T47D
I
shMETTL3: - + + +
siTMEM127: - - 1 2
TMEM127
p-S6K
S6K
METTL3
Vinculin
T47D
J
T47D
shCtrl
shMETTL3
shMETTL3+siTMEM127-1
shMETTL3+siTMEM127-2
OD value
1.5
1.0
0.5
0.0
***
***
0
2
4
6
Days

Figure 7

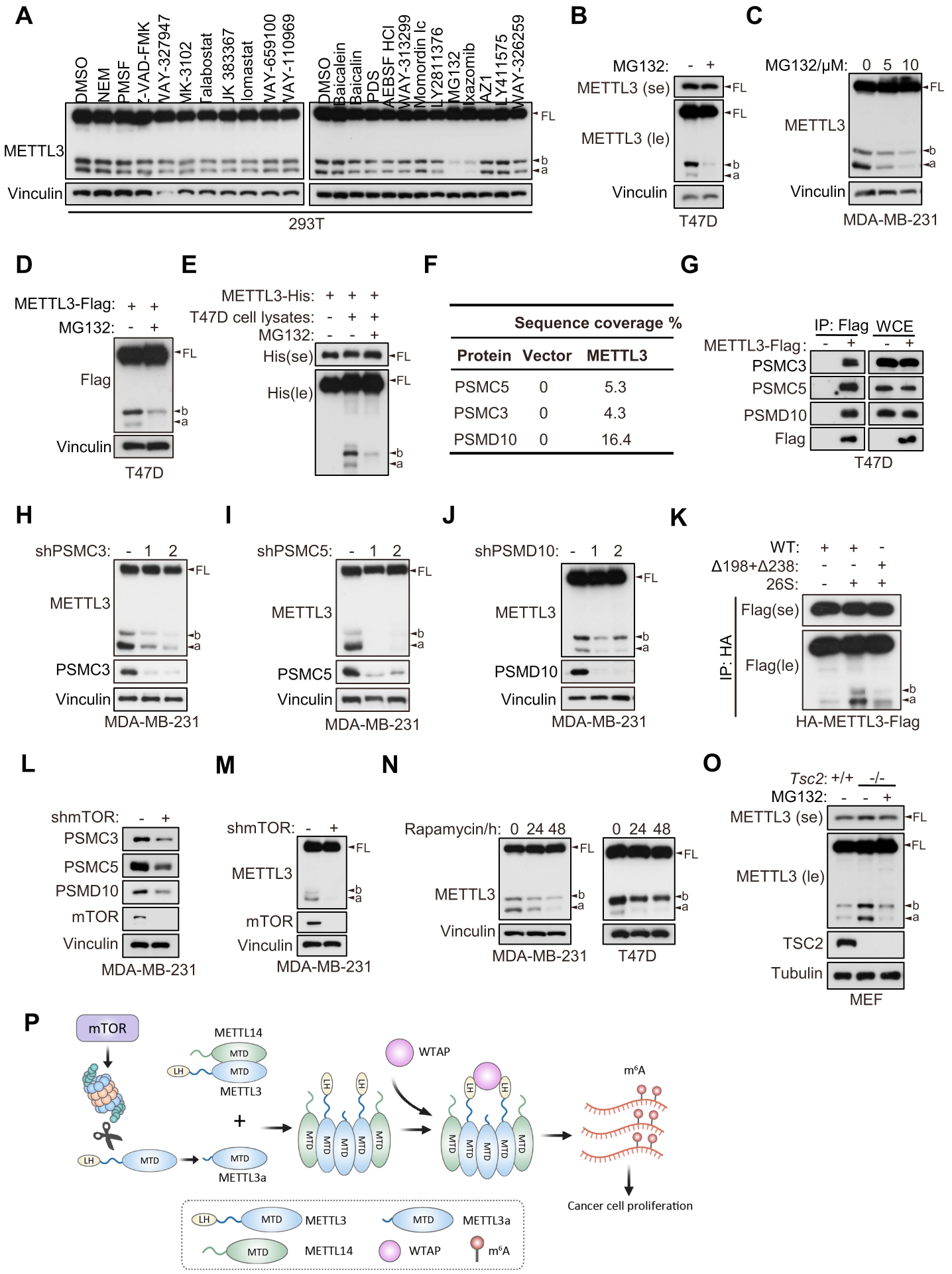
A
DMSO
NEM
PMSF
Z-VAD-FMK
WAY-327947
MK-3102
Talabostat
UK 383367
Ilomastat
WAY-659100
WAY-110969
DMSO
Baicalein
Baicalein
PDS
AEBSF HCl
WAY-313299
Momordin Ic
LY2811376
MG132
Ixazomib
AZ1
LY411575
WAY-326259
METTL3
Vinculin
FL
b
a
293T
B
MG132: - +
METTL3 (se)
METTL3 (le)
Vinculin
T47D
C
MG132/μM: 0 5 10
METTL3
Vinculin
MDA-MB-231
D
METTL3-Flag: + +
MG132: - +
Flag
Vinculin
T47D
E
METTL3-His: + + +
T47D cell lysates: - + +
MG132: - - +
His(se)
His(le)
F
Sequence coverage %
Protein Vector METTL3
PSMC5 0 5.3
PSMC3 0 4.3
PSMD10 0 16.4
G
IP: Flag WCE
METTL3-Flag: - + - +
PSMC3
PSMC5
PSMD10
Flag
T47D
H
shPSMC3: - 1 2
METTL3
PSMC3
Vinculin
MDA-MB-231
I
shPSMC5: - 1 2
METTL3
PSMC5
Vinculin
MDA-MB-231
J
shPSMD10: - 1 2
METTL3
PSMD10
Vinculin
MDA-MB-231
K
WT: + + -
Δ198+Δ238: - - +
26S: - + +
IP: HA
Flag(se)
Flag(le)
HA-METTL3-Flag
L
shmTOR: - +
PSMC3
PSMC5
PSMD10
mTOR
Vinculin
MDA-MB-231
M
shmTOR: - +
METTL3
mTOR
Vinculin
MDA-MB-231
N
Rapamycin/h: 0 24 48
0 24 48
METTL3
Vinculin
MDA-MB-231
T47D
O
Tsc2: +/+ -/-
MG132: - - +
METTL3 (se)
METTL3 (le)
TSC2
Tubulin
MEF
P
mTOR
METTL14
METTL3
METTL3a
LH
MTD
WTAP
m6A
Cancer cell proliferation
METTL3
METTL3a
METTL14
WTAP
m6A

Supplementary Figure 1

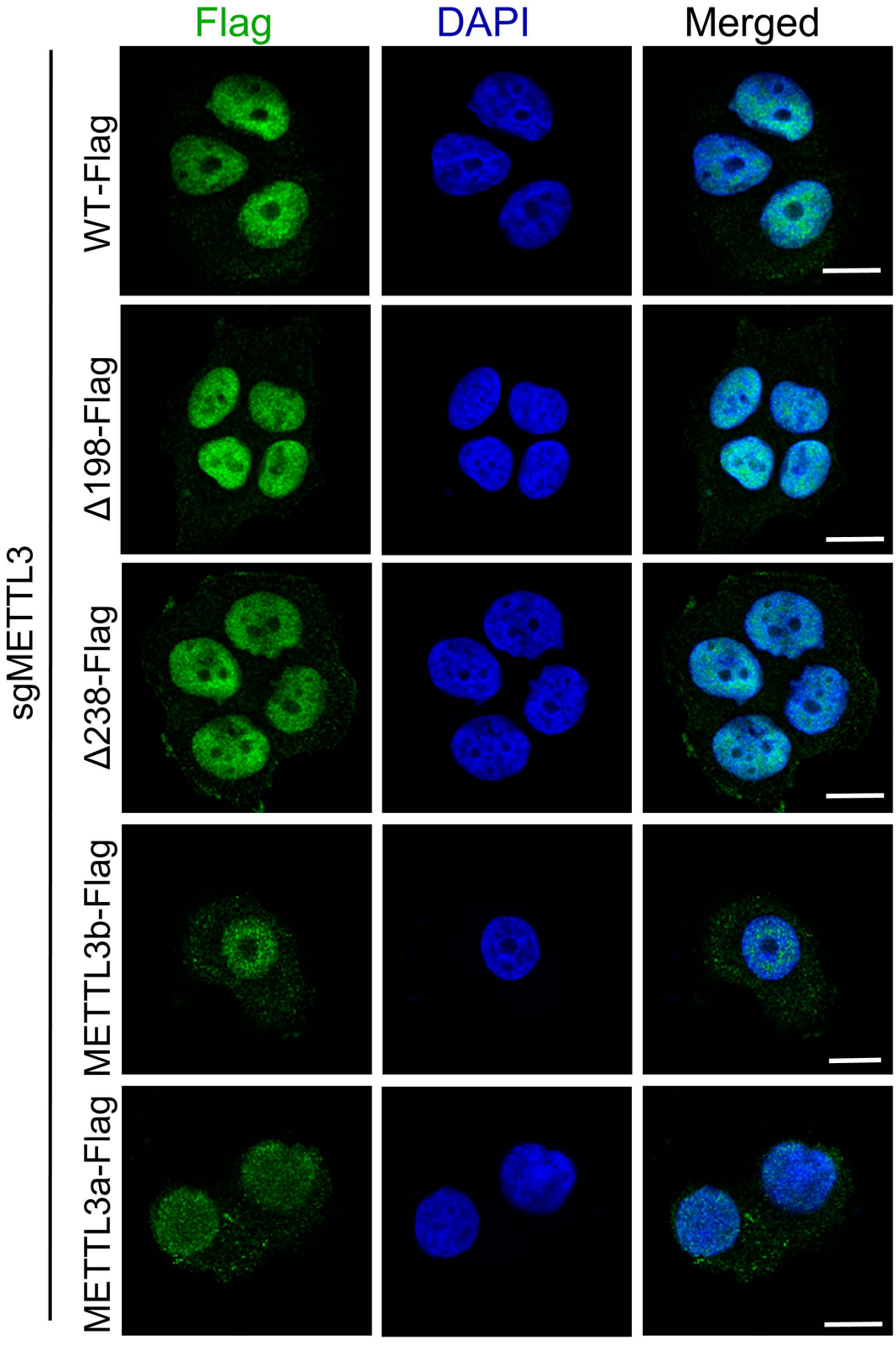

Supplementary Figure 2

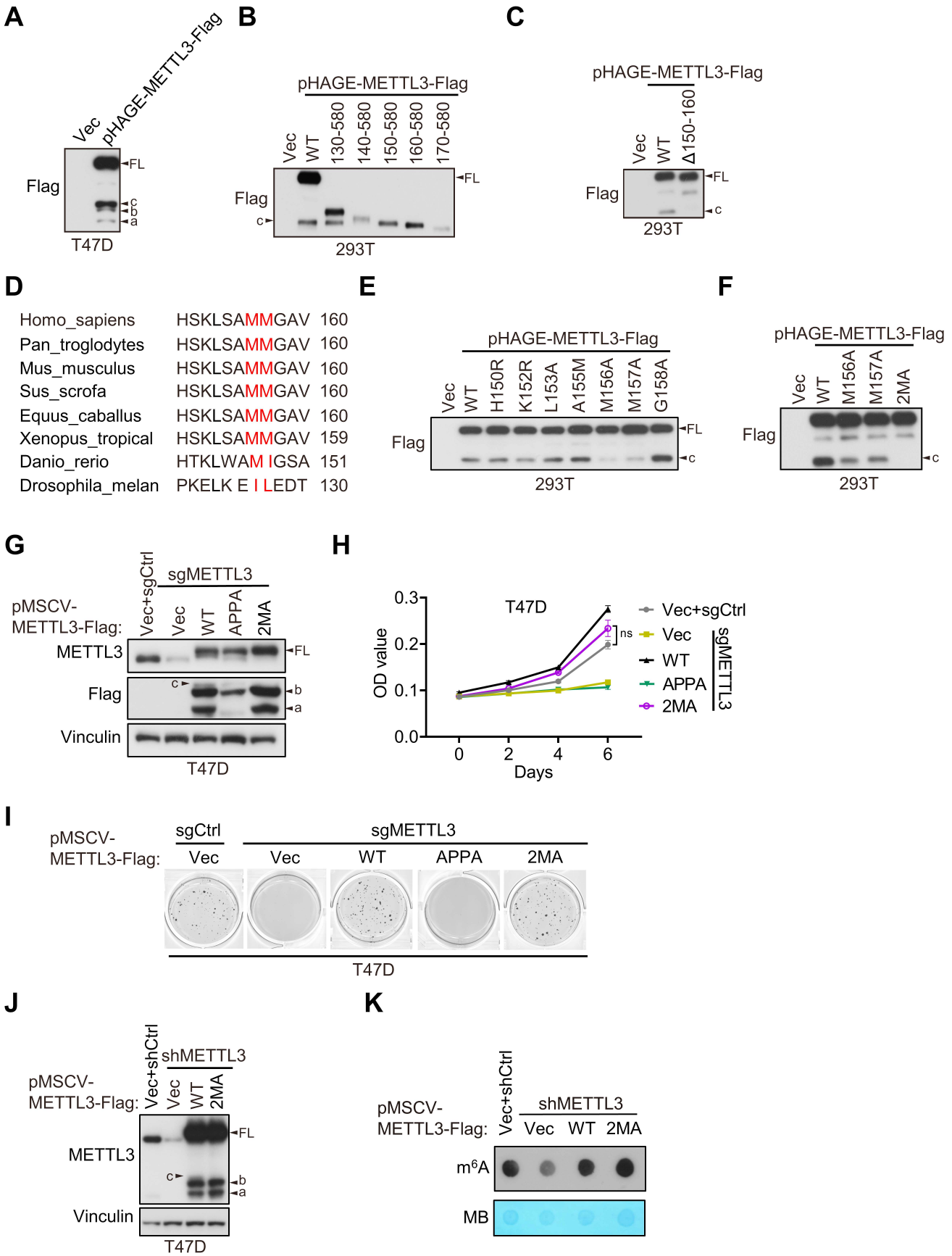

Supplementary Figure 3

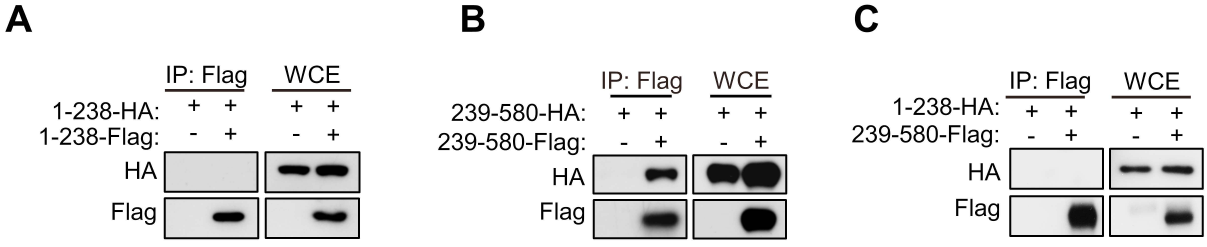

Supplementary Figure 4

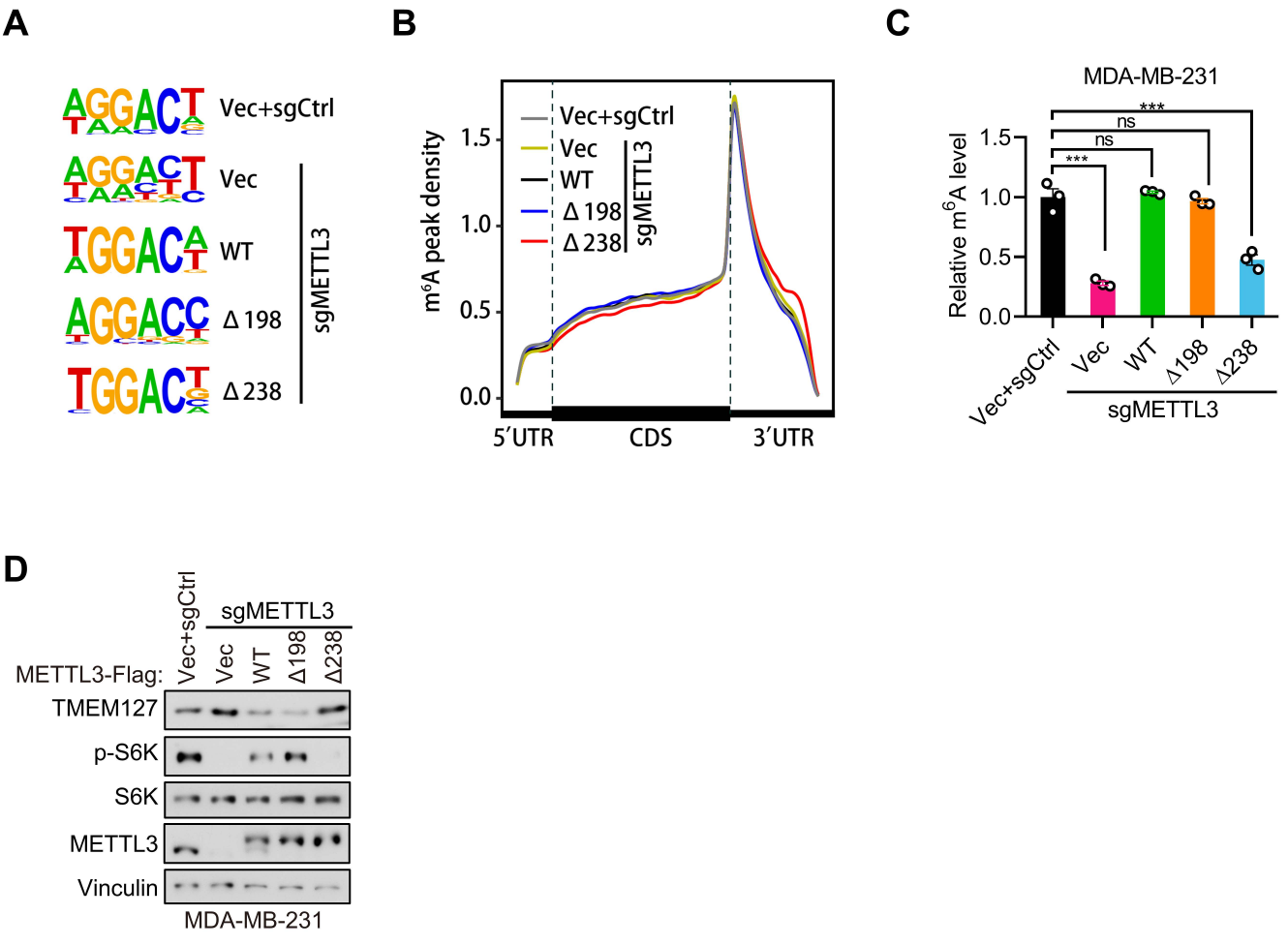

Supplementary Figure 5

A

cat. Number	Name	Target
S3692	N-Ethylmaleimide (NEM)	Cysteine Protease
S3025	PMSF	irreversible serine/cysteine protease
S8102	Z-VAD(OH)-FMK	irreversible pan-caspase inhibitor
P2550	WAY-327947	caspase
S8565	Omarigliptin (MK-3102)	DPP-4
S8455	Talabostat (Val-boroPro, PT-100)	dipeptidyl peptidase
S2224	UK 383367	Procollagen C Proteinase
S7157	Ilomastat (GM6001, Galardin)	MMP
P3183	WAY-659100	hormone sensitive lipase (HSL); metalloprotease
P2039	WAY-110969	tyrosinase
S2268	Baicalein	P450 (e.g. CYP17), endopeptidase
S2269	Baicalin	GABA Receptor, endopeptidase
S7382	Phosphoramidon Disodium Salt (PDS)	endopeptidase
S7378	AEBSF HCl	Serine Protease
P2246	WAY-313299	JAMM protease
S9159	Momordin Ic	SENP1
S1528	LY2811376	non-peptidic β-secretase(BACE1)
S2619	MG-132	proteasome and calpain
S2180	Ixazomib (MLN2238)	20S proteasome
S8904	AZ1	ubiquitin-specific protease (USP) 25/28.
S2714	LY411575	γ-secretase
P2462	WAY-326259	thrombin; factor XIa

B

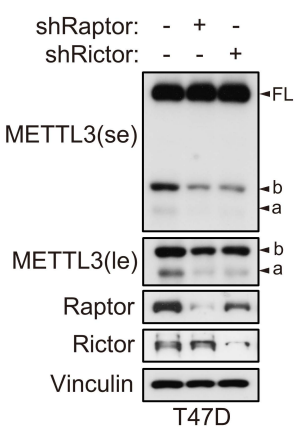
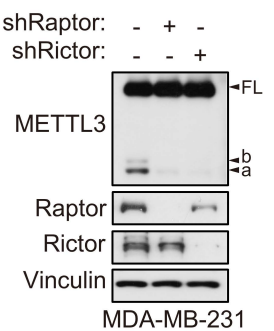
C